

A Historical Review of the Absorbing Boundary Conditions for Electromagnetics

Jean-Pierre Bérenger

School of Electrical and Electronic Engineering

The University of Manchester, UK

(Email: jpberenger@gmail.com)

Abstract—This paper reviews the absorbing boundary conditions (ABCs) used in the past 40-45 years to solve open problems with such numerical techniques as the finite difference or the finite element methods. Numerous ABCs have been proposed over the years in the various domains of Physics. The review is limited to the local ABCs that have been used in numerical electromagnetics, even if some were initially introduced in acoustics. More specifically, the review addresses the ABCs used before 1994, which were mainly analytical ABCs, the Perfectly Matched Layer (PML), used in the past 20 years, and the recently introduced Huygens ABC (HABC). The ABCs are briefly described, with an emphasis on their drawbacks and limitations. A special attention is paid to the absorption of the evanescent waves which is a critical question in the matter of ABCs.

Index Terms— Absorbing Boundary Condition, ABC, PML, Numerical Method, Electromagnetics, FDTD, FEM.

I. INTRODUCTION

When solving the Maxwell Equations with such numerical techniques as the finite difference or the finite element methods, the computational domain is discretized with cells or elements which must be shorter than both the wavelengths of interest and the geometrical details. In consequence, the physical domain where the equations can be solved must be finite. This is inconsistent with most problems of electromagnetism that are unbounded in space. Two examples are the radiation of an antenna in free space and the interaction of an incident wave with a scattering structure.

To overcome the contradictory requirements, the absorbing boundary conditions (ABCs) have been introduced. They replace or simulate the infinite space that surrounds the finite computational domain. They permit the solution to be an acceptable approximation of the solution that would be obtained within a really infinite domain. The accuracy of the approximation depends on the features of the ABC and on many other parameters, and there are some limitations on the simulation of free space with an ABC. Especially, the ABC cannot replace sources which are outside it. When physical sources are outside the ABC, they must be replaced with

equivalent sources inside the ABC or with a boundary condition combined with the ABC. The ABCs reviewed in this document are only the time domain ABCs. However, most can also be expressed in frequency domain form and can then be used with such frequency domain methods as the finite elements or the parabolic equation. The review is also limited to the local ABCs. There exist global ABCs where the field on the boundary is estimated in function of the field in the whole computational domain, but their computational cost is high and they are rarely used in time domain methods.

There is a need of ABCs only with finite methods. With such other methods as the integral equation methods, there is no need of ABC. Because the equations to be solved are equivalent to the Maxwell equations, the boundary conditions, and the initial conditions. The infinity of space is then implicit. For this reason, the need of ABCs appeared only when the computers became able to handle finite method resolutions. The first paper in the literature opening the way to such a possibility was probably the one of K.S. Yee in 1966 [1], which presents the FDTD method. There is no ABC in this paper, but it is evident as reading it that the FDTD method is limited to finite domains, which implicitly suggests that something must be done to apply the method to the numerous problems of electromagnetism where the physical domain is not bounded by enforced boundary conditions. The first paper that reported the use of the FDTD method to solve an unbounded two-dimensional (2D) problem was published by Merewether in 1971 [2]. The ABC was the “radiating boundary”, later used in 3D by Holland [3].

After the Merewether work, numerous ABCs appeared in the literature. Schematically, there has been three periods in the development of ABCs. The first period, from 1971 to 1994, where several ABCs were introduced in acoustics and in electromagnetics. Most are analytical ABCs, which means that the field on the outer boundary is computed by a certain formula in function of the field at some locations in the interior of the domain. The second period, from 1994 to the years 2000’s, followed the introduction of the Perfectly Matched Layer (PML) [4]. Because of its far better performance than that of previous ABCs, during this period almost all the works on ABCs were focused on the PML. In the third period, corresponding roughly to the past 10 years, other ABC ideas have been proposed in the literature. Some

are of interest and lead to ABCs that can challenge the PML, at least in some situations.

This review is composed of three parts that correspond to the three periods of the ABC developments. Firstly the analytical ABC period, up to 1994, second the PML period, and third the recent period where new ideas emerged. The different ABCs are briefly described with a special emphasis on their drawbacks and limitations. In particular, the question of the absorption of the evanescent fields by the ABCs is discussed. This is a critical question that explains why some ABCs perform better than others.

II. THE ABSORBING BOUNDARY CONDITIONS IN THE 1970 AND 1980 YEARS

The need of ABCs appeared at the beginning of the 70's when the computer technology permitted finite difference methods to be used. In electromagnetics, the FDTD method [1] was used initially for the calculation of the coupling of the nuclear electromagnetic pulse (NEMP) to structures. This is a typical problem where an ABC is needed. NEMP coupling then played a capital role in the development of ABCs. In the USA, the radiating boundary ABC described in 2D in 1971 [2] and in 3D in 1977 [3] was probably the most used ABC in the early NEMP works. In France, use of FDTD also began with NEMP studies, in 1976. To this end, the matched layer (ML) ABC was developed [5, 6]. The ML was probably used as well by some workers in the USA since its use was also reported in [7].

Several analytical ABCs were introduced in the 70's and 80's. Most for the acoustic waves, but they could be applied to electromagnetic waves as well. The most known are the Engquist-Majda one-way wave equations [8], and the Higdon operators [9, 10]. Among others some are the Bayliss and Turkel condition [11], the Reynolds condition [12], the Keys condition [13], and the Liao condition [14], which are reviewed in the following.

II-1. A simple and intuitive ABC for traveling waves

A common feature to most analytical conditions is the assumption that the waves to be absorbed are traveling waves propagating with the speed of light c . In such conditions, an intuitive and simple ABC can be derived. Assuming that the propagation is in x direction perpendicular to the boundary, traveling waves can be expressed in the form

$$E(x, t) = f_E(t - x/c) \quad (2-1)$$

where E is the electric field, f_E is a function of a single variable, and t is the time. Deriving (2.1) with respect with x and t shows that the waves $E(x, t)$ also satisfy the equation

$$\frac{\partial E}{\partial x} + \frac{1}{c} \frac{\partial E}{\partial t} = 0 \quad (2-2)$$

From (2-1), the field on the boundary at a given time t is the field that was present at the location Δb from the boundary at time $t - \Delta t$, where Δb is the distance of propagation during Δt , that is $\Delta b = c \Delta t$. This is schematized in Fig. 2-1 and can be written as

$$E(x_b, t) = E(x_b - \Delta b, t - \Delta t) \quad (2-3)$$

where x_b is the x coordinate of the boundary. Using (2-3) as a boundary condition the absorption is perfect for the plane waves at normal incidence. But for any other incidence it produces a reflection which can be easily predicted. To do this, let us consider a plane wave E_i striking the boundary at incidence θ , with the corresponding reflected wave E_r (Fig. 2-2). Setting $x = x_b = 0$ on the boundary, they can be written as

$$E_i(x, y, t) = E_{0i} e^{j\omega t - jk_x x - jk_y y} \quad (2-4)$$

$$E_r(x, y, t) = E_{0r} e^{j\omega t + jk_x x - jk_y y} \quad (2-5)$$

where $k_x = \omega \cos\theta/c$ and $k_y = \omega \sin\theta/c$ are the wavenumbers in x and y directions.

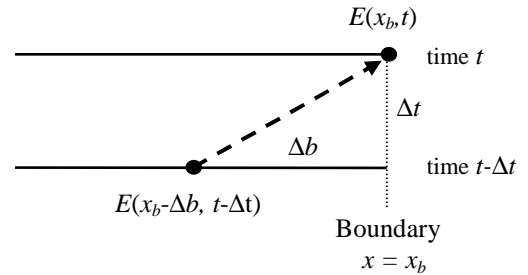


Fig. 2-1. Field on the boundary at current time t in function of the field at previous time $t - \Delta t$.

Enforcing condition (2-3) on the boundary means that the sum of the two waves satisfies (2-3). This yields

$$E_{0i} e^{j\omega t} + E_{0r} e^{j\omega t} = E_{0i} e^{j\omega(t - \Delta t) + jk_x \Delta b} + E_{0r} e^{j\omega(t - \Delta t) - jk_x \Delta b} \quad (2-6)$$

Assuming in addition that Δb is small with respect to the wavelength, the exponentials can be replaced with their first order expansion, which yields

$$E_{0i} + E_{0r} = E_{0i} (1 - j\omega \Delta t + jk_x \Delta b) + E_{0r} (1 - j\omega \Delta t - jk_x \Delta b) \quad (2-7)$$

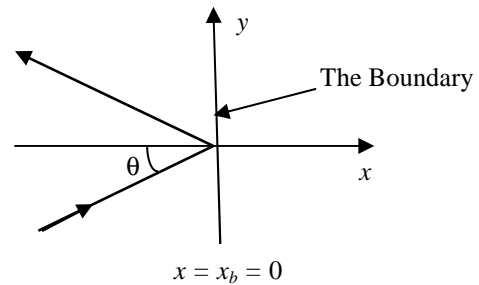


Fig. 2-2. A plane wave at incidence θ on the plane boundary.

From which, using $\Delta t = \Delta b/c$, the reflection coefficient $r = E_{0r}/E_{0i}$ is,

$$r = \frac{k_x - \omega/c}{k_x + \omega/c} \quad (2-8)$$

or, since $k_x = \omega \cos\theta/c$:

$$r = \frac{\cos\theta - 1}{\cos\theta + 1} \quad (2-9)$$

The reflection is shown in Fig. 2-3 (the traveling wave curve). As expected it vanishes at $\theta = 0$, but it is total at grazing incidence, and equals 17 % at 45° . It should be noticed that the reflection (2-8) can also be obtained by enforcing the sum of waves (2-4) and (2-5) into equation (2-2). The discrete equation (2-3) is consistent with the partial derivative equation (2-2).

Reflection (2-9) has been derived for pure traveling waves. Consider now evanescent waves. It is also possible to derive the reflection coefficient. The plane wave solutions of the Maxwell Equations whose phase propagates in direction θ of the (x, y) plane and whose magnitude is evanescent in the direction $\theta + \pi/2$, can be written in the form (2-4), but with wavenumbers (see Appendix A)

$$k_x = \frac{\omega}{c} (\cosh \chi \cos \theta + j \sinh \chi \sin \theta) \quad (2-10)$$

$$k_y = \frac{\omega}{c} (\cosh \chi \sin \theta - j \sinh \chi \cos \theta) \quad (2-11)$$

where χ is the evanescence coefficient. Traveling waves are the special case $\chi = 0$. The reflected wave remains in the form (2-5) because it propagates in direction $\pi - \theta$ and its χ coefficient is of opposite sign (see Appendix A). The derivation (2-6)-(2-8) then remains valid. Using (2-10) and (2-11) into (2-8) yields

$$r = \frac{\cosh \chi \cos \theta - 1 + j \sinh \chi \sin \theta}{\cosh \chi \cos \theta + 1 + j \sinh \chi \sin \theta} \quad (2-12)$$

which obviously reduces to (2-9) when $\chi = 0$. For any other value of χ , the reflection does not vanish at normal incidence. For example, $r(0) = 1/3$ with $\cosh \chi = 2$. And for strongly evanescent waves ($\cosh \chi \gg 1$), the reflection is total ($r = 1$) for any θ . The reflection is plotted in Fig. 2-3 for $\cosh \chi = 1.5, 3$, and 10.

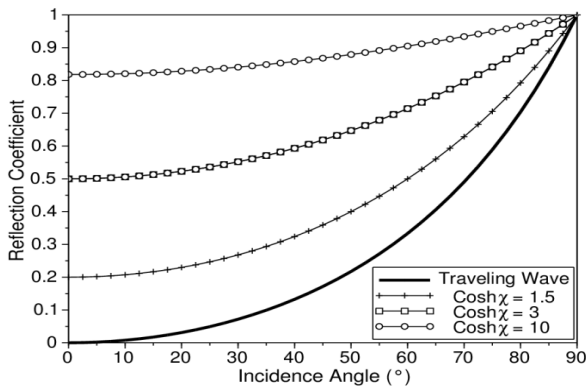


Fig. 2-3. Reflection coefficient r for a traveling wave and for three evanescent waves of $\cosh \chi = 1.5, 3$, and 10.

In summary, by assuming that the waves are pure traveling waves, boundary conditions can be easily found, in the continuous (2-2) or discrete (2-3) forms. They can well absorb the traveling waves, at least at incidences close to the normal incidence. But the evanescent waves are poorly absorbed, especially the strongly evanescent ones which are reflected in totality at any incidence angle. The analytical ABCs reviewed

in the following also assume that the outgoing waves are traveling waves. Despite that they are derived using more mathematics, in their first order versions they are actually equivalent to the above intuitive ABC (2-2) or (2-3). And their more sophisticated high order versions can be viewed as successive applications of the first order versions. From this, they also suffer from the drawback summarized in Fig. 2-3, i.e. they strongly reflect the evanescent waves.

II-2. The Engquist-Majda ABC

Engquist and Majda [8] derived a family of ABC's from the second order wave equation, which reads, by assuming invariance in z direction:

$$\frac{1}{c^2} \frac{\partial^2 E}{\partial t^2} = \frac{\partial^2 E}{\partial x^2} + \frac{\partial^2 E}{\partial y^2} \quad (2-13)$$

Inserting a plane wave propagating in direction θ , in the form (2-4), yields the equation of dispersion

$$\omega^2 / c^2 = k_x^2 + k_y^2 \quad (2-14)$$

which can be rewritten using $k_y = \omega \sin \theta / c$

$$k_x = \pm \frac{\omega}{c} \sqrt{1 - \sin^2 \theta} \quad (2-15)$$

Quantity $\sin^2 \theta$ is small v.s. one, as long as θ is not too large. This suggests using an approximation of the square root. The simplest reads, by retaining the + sign

$$k_x = \omega / c \quad (2-16)$$

which can be rewritten as

$$j k_x = \frac{j \omega}{c} \quad (2-17)$$

Using the derivatives of waveform (2-4) shows that (2-17) is nothing but the equation of dispersion of the time domain equation (2-2), which is then the first order Engquist-Majda equation. Using it as a boundary condition produces the reflection (2-9).

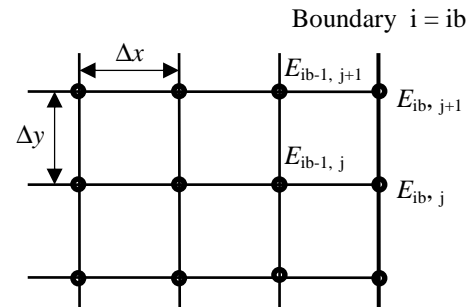


Fig. 2-4. Finite difference grid.

Using (2-2) as an ABC in a finite method consists in discretizing it in order to permit E to be computed on the boundary in function of E at inner nodes and, or, at previous time steps. Consider the finite difference method (FDTD) with nodes separated with Δx and Δy in space (Fig. 2-4), sampled in time with step Δt . The discrete values of E are computed at nodes (i, j) and at times n . The discrete condition (2-3) is consistent with (2-2), but it cannot be applied as it stands since

in general Δb is not a multiple of the step Δx . Interpolations would be needed to enforce (2-3). A discrete condition that can be used with any step Δx can be obtained [8] by a finite difference approximation of (2-2). More precisely, by discretizing the derivatives on space and time in (2-2) at location $\Delta x/2$ from the boundary, and at an intermediate time between n and $n+1$ (called the “box” discretization). This permits use of centred derivatives in space and time. With usual notations of the FDTD method, this reads:

$$\frac{(E_{ib,j}^n + E_{ib,j}^{n+1})/2 - (E_{ib-1,j}^n + E_{ib-1,j}^{n+1})/2}{\Delta x} + \frac{1}{c} \frac{(E_{ib-1,j}^{n+1} + E_{ib,j}^{n+1})/2 - (E_{ib-1,j}^n + E_{ib,j}^n)/2}{\Delta t} = 0 \quad (2-18)$$

from which the unknown E field at time $n+1$ on the boundary is found in function of known fields:

$$E_{ib,j}^{n+1} = E_{ib-1,j}^n + w E_{ib-1,j}^{n+1} - w E_{ib,j}^n \quad (2-19)$$

where

$$w = \frac{c \Delta t - \Delta x}{c \Delta t + \Delta x} \quad (2-20)$$

As expected, it can be easily verified by inserting (2-4) and (2-5) into (2-19) that its reflection coefficient is (2-9) for traveling waves, and (2-12) for evanescent waves.

Higher order approximations of the square root in (2-15) yield higher order ABCs. The second order is obtained by using the first order Taylor approximation:

$$k_x = \frac{\omega}{c} \left(1 - \frac{1}{2} \sin^2 \theta \right) \quad (2-21)$$

that can be rewritten using $k_y = \omega \sin \theta / c$

$$-\omega^2 + \omega c k_x = -c^2 \frac{1}{2} k_y^2 \quad (2-22)$$

From the second derivatives of (2-4), this is the equation of dispersion of:

$$\frac{\partial^2 E}{\partial t^2} + c \frac{\partial^2 E}{\partial x \partial t} = \frac{1}{2} c^2 \frac{\partial^2 E}{\partial y^2} \quad (2-23)$$

which is the second-order Engquist-Majda equation [8]. It should be noticed that (2-23) has been derived here assuming invariance in z direction. For a true 3D case, the other transverse derivative, i.e. $\delta^2 E / \delta z^2$, must be added to $\delta^2 E / \delta y^2$ in (2-23).

The reflection coefficient of (2-23) can be obtained as previously by enforcing the sum of (2-4) and (2-5). This yields, for the traveling waves

$$r = - \left(\frac{\cos \theta - 1}{\cos \theta + 1} \right)^2 \quad (2-24)$$

which is just the square of (2-9). The second order equation (2-23) allows then a better absorption of the traveling waves. At $\theta = 45^\circ$ the reflection is about 3% in place of 17%. For the evanescent waves, enforcing (2-4) and (2-5) with (2-10) and (2-11) into (2-23) yields

$$r = - \left(\frac{\cosh \chi \cos \theta - 1 + j \sinh \chi \sin \theta}{\cosh \chi \cos \theta + 1 + j \sinh \chi \sin \theta} \right)^2 \quad (2-25)$$

which is also the square of the first order reflection (2-12).

The finite difference discretization of (2-23) can be found in [15] or in textbooks [16, 17]. A third order equation was also derived in [8] using a Pade approximation of the square root, achieving a reflection equal to the cube of (2-9). Later, Halpern and Trefelthen [18] derived other equations by using other approximations of the square root, such as least-squares or interpolation at Chebyshev or Neuman points. These approximations permit the angle of exact absorption (where $r = 0$) to be shifted to non zero angles (two angles where $r = 0$ for the second order equation). This improves the absorption at wide angles. Discussions and experiments on the effect of the choice of the approximation can be found in [19, 20]. However, whatever may be their order and their complexity, all the approximations only considered the absorption of traveling waves. This means that evanescent waves are reflected, partially or in totality, depending on their evanescence coefficient. This is why in electromagnetics, where there are always evanescent fields, the absorption was not significantly improved by using Engquist-Majda equations of order higher than two. For a decade, up to 1994, the most used ABC has been the second order ABC (2-23), with its FDTD implementation in [15], known as the Mur ABC. The Engquist-Majda ABC has been also used in frequency domain form with the finite element method [60].

II-3. The Higdon ABC

The theory of the Higdon operators was presented in two papers [9, 10]. Conversely to the Engquist-Majda ABCs, which are analytical approximations of the wave equation that are discretized for application to finite methods, the Higdon operators are directly defined in the discrete space. Higdon first defines two operators, K and Z^{-1} , which shift backward the physical quantity, by one space step and one time step, respectively. In electromagnetics, this reads, for the E field:

$$K E_{i,j}^n = E_{i-1,j}^n \quad \text{and} \quad Z^{-1} E_{i,j}^n = E_{i,j}^{n-1} \quad (2-26)$$

where i is the index of the mesh in the direction of the space shift perpendicular to the boundary. He then considers operators composed of the addition of the identity operator with a polynomial combination of K and Z^{-1} , in the form:

$$B(K, Z^{-1}) = I - \alpha_1 K - \alpha_2 Z^{-1} - \alpha_3 K Z^{-1} - \alpha_4 K^2 - \alpha_5 Z^{-2} - \dots \quad (2-27)$$

where K^m and Z^n mean that the shifts are applied m and n times (shifts by $m \Delta x$ or $n \Delta t$). Applying $B(K, Z^{-1})$ to the unknown field value on the boundary $E_{ib,j}^{n+1}$

$$B(K, Z^{-1}) E_{ib,j}^{n+1} = 0 \quad (2-28)$$

gives $E_{ib,j}^{n+1}$ in function of E at interior nodes of the grid ($i < ib$) at time $n+1$ and at nodes ($i \leq ib$) at previous times.

Consider for instance the operator

$$B_1(K, Z^{-1}) = I - K Z^{-1} - w K + w Z^{-1} \quad (2-29)$$

with w from (2-20). Its application to $E_{ib,j}^{n+1}$ yields (2-19). The first order Engquist-Majda approximation can be viewed as a Higdon operator. This operator is then consistent with the equation (2-2). And its reflection coefficient is (2-9) for traveling waves, and (2-12) for evanescent waves.

An important result of the Higdon papers is the possibility of multiplying the operators, where the multiplication is defined as with polynomials. Then, the reflection coefficient of the resulting operator is the product of the reflections of the two operators. This permits easy design of high order operators with desired features by combining low order operators. In fact, in his paper [10], Higdon considers the operator (2-29) with the following quantity w :

$$w = \frac{c \Delta t - \cos \theta_0 \Delta x}{c \Delta t + \cos \theta_0 \Delta x} \quad (2-30)$$

Then, (2-29) corresponds to the discretization of the continuous equation

$$\frac{\partial E}{\partial x} + \frac{\cos \theta_0}{c} \frac{\partial E}{\partial t} = 0 \quad (2-31)$$

The interest of the introduction of $\cos \theta_0$ is that the reflection is no longer (2-9), it becomes

$$r = \frac{\cos \theta - \cos \theta_0}{\cos \theta + \cos \theta_0} \quad (2-32)$$

that vanishes at the angle $\theta = \theta_0$ in place of $\theta = 0$. An operator of order p can be obtained by multiplying p operators (2-29) with different angles of zero reflection θ_0

$$B_p(K, Z^{-1}) = \prod_{j=1}^p (I - K Z^{-1} - w_j K + w_j Z^{-1}) \quad (2-33)$$

where the w_j are given by (2-30) with the desired θ_{0j} . The reflection is then the product of p reflections (2-32). This p -order operator is consistent with the continuous equation

$$\prod_{j=1}^p \left(\frac{\partial}{\partial x} + \frac{\cos \theta_{0j}}{c} \frac{\partial}{\partial t} \right) E = 0 \quad (2-34)$$

In practice of electromagnetics, the operator that was used was the second order one ($p = 2$), which reads, from (2-33):

$$\begin{aligned} B_2(K, Z^{-1}) = & I - (w_1 + w_2) K + w_1 w_2 K^2 \\ & + (w_1 + w_2) Z^{-1} - 2(1 + w_1 w_2) K Z^{-1} + (w_1 + w_2) K^2 Z^{-1} \\ & + w_1 w_2 Z^{-2} - (w_1 + w_2) K Z^{-2} + K^2 Z^{-2} \end{aligned} \quad (2-35)$$

The expression of E^{n+1} on the boundary follows immediately by using (2-35) into (2-28). With the FDTD method, in general w_1 and w_2 were chosen such that $\theta_{01} = \theta_{02} = 0$, with then reflection coefficient (2-24)-(2-25).

What should be noticed is that the second order Higdon ABC only needs field values at nodes located on the line normal to the boundary. Conversely to the discretization of Engquist-Majda (2-23) where values at nodes out of this line are needed due to the second order derivative in direction parallel to the boundary. This is an advantage of Higdon ABC

in the edges of computational domains where (2-23) cannot be used and must be replaced with the first order (2-2).

Since the theoretical reflection from the Higdon operator is the same as that from the Engquist-Majda ABC, at least when all the zero reflection angles θ_j equal zero, the performances of the two ABCs are quite similar, which means good absorption of traveling waves, but strong reflection of evanescent fields in both cases.

II-4. Other analytical ABCs

The first ABC reported in the literature is probably the *radiating boundary* [2, 3]. It consists in estimating the field on the boundary in function of the field at inner nodes assuming it varies as

$$E(R, t) = \frac{E(t - R/c)}{R} \quad (2-36)$$

where R is the distance from a point somewhere in the center region of the computational domain. Obviously, this field form comes from the behavior of the field radiated far away from such sources as antennas or scattering structures. The form (2-36) is close to (2-1) with in addition the coefficient $1/R$ to take account that the field decreases with distance. Also, the estimate relies on field values located on lines from the current node on the boundary to the center of the domain, instead of on lines perpendicular to the boundary. In principle, this could be more accurate than the first order Mur or Higdon ABCs, because of the better match of the physical field by the assumed evolution (2-36) in many problems. However, the implementation was complicated, especially in 3D [3]. And it seems that this ABC suffered from late time instability [21]. And, as Mur or Higdon ABCs, the absorption of evanescent fields was not addressed, which probably explains why the ABC had to be placed some distance from the scattering structure, as reported in [3].

Another ABC used in the early times of the FDTD method was that used by *Taflove* in his pioneering work on bioelectromagnetism [22, 23]. On the boundary he enforced the average of the fields that were present at the closest interior three nodes two time steps before. If only the closest node were used, since he worked with $2 c \Delta t = \Delta x$ the condition would be exact for plane waves at normal incidence, like with the ABC schematized in Fig. 2-1. The averaging removes the exactness at normal incidence, but probably improves the absorption at wide angles.

The *Bayliss and Turkel condition* [11] is an ABC introduced in 1980 for electromagnetics. It can be viewed as an improved Merewether ABC. It also relies on the decrease of the field with distance from a radiating object, but it uses more sophisticated waveforms. Instead of (2-36) it uses the expansion of the field with a series of terms decreasing as the powers of $1/R$. Operators that annihilate the outgoing field are derived, with different orders of approximation. The method is in principle more accurate than that of Merewether, but it is also expressed in spherical coordinates, so that its implementation in a FDTD Cartesian grid is not natural and complicated. Its use on a circular boundary in the frequency domain FEM is reported in [60]. As Engquist-Majda and Higdon ABCs, the Bayliss and Turkel ABC only addresses

traveling field and then cannot work properly in the vicinity of sources where evanescent fields are present.

The *Reynolds ABC* [12], published in 1978, is interesting because it connects the Engquist-Majda ABC, published in 1977, with the future Higdon ABC, published in 1986. In fact, the operator (2-29), generally known as the Higdon operator, was previously used in the work of Reynolds. By reasoning as in the above section 2.1 he derived the first order equation (2-2) and its reflection coefficient (2-9). Then through a relatively complex derivation where a square root is approximated, he arrived at the following approximation of the wave equation

$$\frac{1}{c} \frac{\partial^2 E}{\partial x \partial t} + \frac{\partial^2 E}{\partial x^2} + \frac{1}{2} \frac{\partial^2 E}{\partial y^2} = 0 \quad (2-37)$$

He could not obtain stable finite difference approximation to (2-37) and then replaced the second order derivative in the transverse direction y using (2-13). This gives:

$$\frac{1}{c^2} \frac{\partial^2 E}{\partial t^2} + \frac{2}{c} \frac{\partial^2 E}{\partial x \partial t} + \frac{\partial^2 E}{\partial x^2} = 0 \quad (2-38)$$

which can be rewritten as

$$\left(\frac{\partial}{\partial x} + \frac{1}{c} \frac{\partial}{\partial t} \right) \left(\frac{\partial}{\partial x} + \frac{1}{c} \frac{\partial}{\partial t} \right) E = 0 \quad (2-39)$$

We firstly notice that (2-39) is nothing but the second order Higdon equation, i.e. (2-34) with $p=2$ and $\theta_0=0$. Secondly, using the wave equation (2-13) to eliminate $\delta^2 E / \delta^2 x$, equation (2-38) becomes (2-23). All this shows that the second order Engquist-Majda equation, the second order Reynolds equation, and the second order Higdon operator, are consistent and correspond to the same approximation of the wave equation. This can also be viewed by deriving (2-37) or (2-38) from (2-22) which is the equation obtained by approximating the square root in (2-15). For (2-38) for example, (2-22) can be rewritten, by replacing k_y with k_x :

$$-\frac{1}{2} \frac{\omega^2}{c^2} + \frac{\omega}{c} k_x - \frac{1}{2} k_x^2 = 0 \quad (2-40)$$

This is the equation of dispersion of (2-38), which is then obtained with the same approximation of (2-15) as that used in the derivation of the Engquist-Majda equation (2-23). And consequently the Higdon operator (2-39) also can be viewed as derived from the same approximation. Reading [12], it can be noticed that Reynolds introduced a parameter p in (2-37) which is then present in one parenthesis of (2-39) where $1/c$ is replaced with p/c . In fact, this parameter is equivalent to the $\cos\theta_0$ in the Higdon equation (2-31). It cancels the reflection for $\cos\theta = p$, as can be verified in the table in [12].

The *Keys absorbing equations* [13] are another approximation of the wave equation and can be derived in a similar way as the Engquist-Majda equations, by starting from (2-14). To this end, let us rewrite (2-14) as

$$\omega/c - \sqrt{k_x^2 + k_y^2} = 0 \quad (2-41)$$

and let us assume that :

$$\sqrt{k_x^2 + k_y^2} = \lambda k_x + \mu k_y \quad (2-42)$$

This gives

$$\omega/c - \lambda k_x - \mu k_y = 0 \quad (2-43)$$

Using the derivatives of (2-4), this is the equation of dispersion of

$$\lambda \frac{\partial E}{\partial x} + \mu \frac{\partial E}{\partial y} + \frac{1}{c} \frac{\partial E}{\partial t} = 0 \quad (2-44)$$

which differs from the first order Engquist-Majda equation (2-2) by the presence of derivatives in both x and y directions. Using $k_x = \omega \cos\theta/c$ and $k_y = \omega \sin\theta/c$ shows that (2-42) is true only for the two angles θ_1 and θ_2 that satisfy $\lambda \cos\theta + \mu \sin\theta = 1$. For these angles, (2-44) is exact. By expressing λ and μ in function of θ_1 and θ_2 , it is possible to arrive at the first order equation of Keys [13], which reads

$$\cos\theta_n \frac{\partial E}{\partial x} + \sin\theta_n \frac{\partial E}{\partial y} + \frac{\cos\theta_0}{c} \frac{\partial E}{\partial t} = 0 \quad (2-45)$$

where

$$\theta_n = \frac{\theta_1 + \theta_2}{2} \quad ; \quad \theta_0 = \frac{\theta_2 - \theta_1}{2} \quad (2-46)$$

By using (2-45) as a boundary equation, the reflection vanishes for incidences θ_1 and θ_2 where (2-45) is exact. The two angles can be chosen at will using (2-46). A higher order equation can also be derived in the same way [13], starting from the following approximation of (2-41):

$$\left(\omega/c - \lambda_1 k_x - \mu_1 k_y \right) \left(\omega/c - \lambda_2 k_x - \mu_2 k_y \right) = 0 \quad (2-47)$$

There is no detail in Keys paper on how (2-45) can be implemented in a finite difference method. And apparently the Keys equations have never been used in electromagnetics.

The *Liao extrapolation ABC* [14] is a condition which relies on another principle. It does not assume that the waves are traveling waves propagating with the speed of light. Instead, it only relies on extrapolation of the field. For each node of the boundary where the field has to be predicted, a Newton backward-difference polynomial is found from values of the field at a set of nodes located on the line normal to the boundary, at previous time steps. Usually, such a polynomial is used to interpolate between values used to find its coefficients. Here it is used to extrapolate the field on the boundary at the desired future time. This results in an ABC which is claimed as more effective than the second order Higdon or Mur ABCs. This may be due to the fact that it is not assumed that the outgoing waves are purely traveling waves. From this, the absorption of evanescent waves may be better than with Mur or Higdon ABCs. There is no sufficient experiment in the literature to clearly conclude on this issue. The Liao extrapolation suffers from instability, but it seems an effective remedy was found consisting in the introduction of small losses.

Strictly speaking, the *Mei-Fang superabsorption* [24] is not a new ABC, but rather a technique to improve the effectiveness of existing analytical ABCs with the FDTD method. It consists in computing the future E field on the boundary and the future H field half a cell from it by using the ABC as if the H node was on the boundary. Assuming then that the outgoing wave is plane and at normal incidence permits a relationship to be found between the errors of the

two estimates, from which the error produced by the estimate of E on the advance of H with the regular FDTD equation can be eliminated. The H field half a cell from the boundary plays then the role of an exact ABC, for the assumed incident plane wave. In practice, it has been reported a significant improvement to the absorption of the first order and second order Mur ABCs. However, the improvement may not be better than the one that could be obtained by just increasing the order of the original ABC. And the technique relies again on the assumption that the incident waves are traveling waves, which means that it has probably no effect on evanescent fields.

An interesting ABC that was briefly reported in the literature is the *Betz-Mitra ABC* [25]. This is a modified Higdon operator which is designed for absorbing the evanescent fields. To this end, the equation (2-2) which is consistent with the first order operator (2-29) is replaced with

$$\frac{\partial E}{\partial x} + \frac{1}{c} \frac{\partial E}{\partial t} + \alpha = 0 \quad (2-48)$$

whose discretization gives the following operator

$$B_1(K, Z^{-1}) = I - w_1 K Z^{-1} - w_2 K + w_3 Z^{-1} \quad (2-49)$$

where:

$$w_1 = \frac{c \Delta t + \Delta x - \alpha \Delta x \Delta t / 2}{c \Delta t + \Delta x + \alpha \Delta x \Delta t / 2}; \quad w_2 = \frac{c \Delta t - \Delta x - \alpha \Delta x \Delta t / 2}{c \Delta t + \Delta x + \alpha \Delta x \Delta t / 2};$$

$$w_3 = \frac{c \Delta t - \Delta x + \alpha \Delta x \Delta t / 2}{c \Delta t + \Delta x + \alpha \Delta x \Delta t / 2} \quad (2-50)$$

The coefficient α in (2-48) permits the spatial derivative to have a contribution that takes account of the decrease of the magnitude of the field in the direction normal to the boundary, that is to take account of evanescent waves. By enforcing the sum of (2-4) and (2-5) with wavenumbers (2-10) and (2-11) into (2-48), the following reflection is obtained

$$r = \frac{\cosh \chi \cos \theta - 1 + j \sinh \chi \sin \theta + j \alpha / \omega}{\cosh \chi \cos \theta + 1 + j \sinh \chi \sin \theta - j \alpha / \omega} \quad (2-51)$$

which obviously reduces to (2-12) when $\alpha = 0$. We can note that for traveling waves ($\cosh \chi = 1$, $\sinh \chi = 0$) r equals (2-9) at high frequency ($\omega \gg \alpha$) and $r = 1$ at low frequency ($\omega \ll \alpha$). This is not a drawback since (2-49) can be multiplied by the normal first order operator to absorb the traveling waves, as in [25]. For the case where $\theta = 0$ and $\cosh \chi \gg 1$ (strongly evanescent waves), there is no absorption since $r = 1$ (ratio of complex conjugates). A more interesting case is when $\theta = -\pi/2$ which corresponds to the propagation of the phase in direction parallel to the boundary, and the direction of evanescence perpendicular to the boundary (Appendix A). In that case:

$$r = \frac{-1 - j \sinh \chi + j \alpha / \omega}{1 - j \sinh \chi - j \alpha / \omega} \quad (2-52)$$

For strongly evanescent waves, i.e. $\sinh \chi \gg 1$, the reflection is null on condition that $\alpha = \omega \sinh \chi$. It will be seen further in this document that a similar condition must hold as well for cancelling the reflection of evanescent waves by a CFS-PML.

The condition is approximately true for the spectrum of the evanescent waves present in many physical problems [26, 27]. The relation $\alpha = \omega \sinh \chi$ could then be exploited to set the optimum α in the same way as the α parameter of the CFS-PML is optimized [26, 27].

II-5. The complementary operators

The complementary operator ABC was introduced in 1995 by Ramahi [28, 29]. Strictly speaking, this is not a new analytical ABC, but rather a method that permits the reflection from existing ABCs to be dramatically reduced. Its basic principle relies on performing two calculations with complementary ABCs producing opposite reflections. If one calculation produces the field E in the computational domain and the other the field E^c , including opposite spurious reflections from the outer boundary, the reflection-free (say exact) solution can be obtained by averaging the two results:

$$E^{exact} = \frac{E + E^c}{2} \quad (2-53)$$

However, there are challenging questions when applying this idea. Firstly, finding complementary ABCs is not trivial, and secondly the multiple reflections of the field from the different outer boundaries of the computational domain and from the objects inside it render the exactness of (2-53) questionable.

The problem of the complementary ABCs has been solved by Ramahi in an elegant manner. He showed that complementary operators can be designed, based on the Higdon operators. The complementary operators of Ramahi produce opposite reflections in the continuous space as well as in the discrete FDTD space, rigorously. In continuous space, the Ramahi pair of complementary equations that approximate the wave equation on the boundary read

$$\frac{\partial}{\partial x} \prod_{j=1}^p \left(\frac{\partial}{\partial x} + \frac{\cos \theta_{0j}}{c} \frac{\partial}{\partial t} \right) E = 0 \quad (2-54)$$

$$\frac{\partial}{\partial t} \prod_{j=1}^p \left(\frac{\partial}{\partial x} + \frac{\cos \theta_{0j}}{c} \frac{\partial}{\partial t} \right) E = 0 \quad (2-55)$$

They just differ from the Higdon equation (2-34) with the multiplication by the derivatives $\delta/\delta x$ and $\delta/\delta t$. These additional terms permit the reflections to be opposite, rigorously. From the Higdon theory, the reflection is the product of the normal operator with the reflection of the additional operators equivalent to the additional derivatives. Consider for instance the equation $\delta E/\delta x = 0$. Its box discretization, as done with (2-2) in (2-18), yields

$$E_{ib,j}^{n+1} = E_{ib-1,j}^n + E_{ib-1,j}^{n+1} - E_{ib,j}^n \quad (2-56)$$

and similarly, the discretization of $\delta E/\delta t = 0$ gives

$$E_{ib,j}^{n+1} = E_{ib-1,j}^n - E_{ib-1,j}^{n+1} + E_{ib,j}^n \quad (2-57)$$

In terms of operators, the two complementary ABCs can then be written as

$$B_x^p(K, Z^{-1}) = (I - K Z^{-1} - K + Z^{-1}) B_p(K, Z^{-1}) \quad (2-58)$$

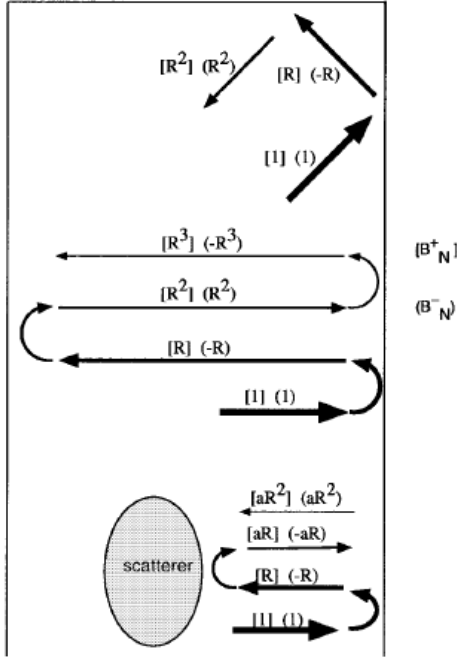


Fig. 1. Multiple reflections due to terminal boundaries, corner regions, and the scatterer (for simplicity, the scatterer is assumed to reflect the field by a factor a).

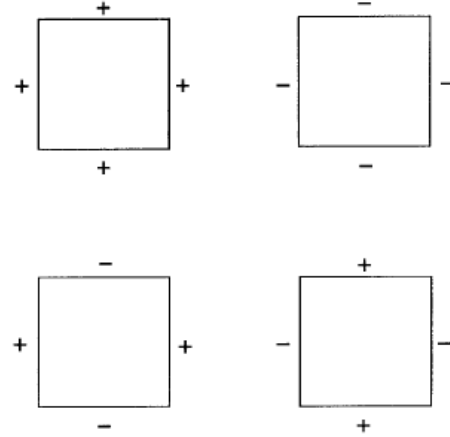


Fig. 2. The four different permutations of boundary operators needed to annihilate corner reflections for 2-D space.

TABLE I
CORNER REGION REFLECTIONS

	1st reflection (R1)	2nd reflection (R2)
solution #1	R	R^2
solution #2	$-R$	R^2
solution #3	R	$-R^2$
solution #4	$-R$	$-R^2$

Fig. 2-5. The various multiple reflections that occur in the computational domain (left-hand part), and the solution proposed by Ramahi to cancel corner reflections in 2D (right-hand part). Source: Ramahi *IEEE Trans. Antennas and Propagation*, vol. 46, pp. 1475-1482, 1998 © 1998 IEEE.

$$B_p^p(K, Z^{-1}) = (I - K Z^{-1} + K - Z^{-1}) B_p(K, Z^{-1}) \quad (2-59)$$

where $B_p(K, Z^{-1})$ is operator (2-33). Using the sum of the incident and reflected waves (2-4) and (2-5) into (2-56) yields the reflection coefficient of the discrete version of the operator $\delta/\delta x$ as:

$$r_x = -\frac{1 - e^{jk_x \Delta x} + e^{-j\omega \Delta t} - e^{jk_x \Delta x} e^{-j\omega \Delta t}}{1 - e^{-jk_x \Delta x} + e^{-j\omega \Delta t} - e^{-jk_x \Delta x} e^{-j\omega \Delta t}} = e^{jk_x \Delta x} \quad (2-60)$$

Similarly, (2-4) and (2-5) into (2-57) give the reflection of the discrete version of $\delta/\delta t$

$$r_t = -\frac{1 + e^{jk_x \Delta x} - e^{-j\omega \Delta t} - e^{jk_x \Delta x} e^{-j\omega \Delta t}}{1 + e^{-jk_x \Delta x} - e^{-j\omega \Delta t} - e^{-jk_x \Delta x} e^{-j\omega \Delta t}} = -e^{jk_x \Delta x} \quad (2-61)$$

The reflections are of opposite signs, as desired, even in the FDTD grid. The operators $\delta/\delta x$ and $\delta/\delta t$ are complementary. They could be used alone to produce opposite reflections of magnitude one. Obviously, one had better to multiply them with another operator that absorbs the waves, as in (2-58) and (2-59) where they are associated with a p -order Higdon operator. Ramahi in his papers produced results with $p = 2$ and $p = 3$.

It should be noticed that with wavenumbers (2-10) and (2-11) of evanescent waves, reflections (2-60) and (2-61) remain valid, i.e. the two operators yield opposite reflections. From this, the operators (2-56) and (2-57) yield reflections -1 and +1 for the evanescent waves. The cancellation effect of (2-53) is then still valid for the evanescent fields. This is a great feature

of the complementary method which permits effective absorption of evanescent fields, as illustrated by several experiments in the papers of Ramahi.

Despite the perfectness of the pair of operators, the basic idea expressed by (2-53) cannot be achieved in a perfect manner because of the multiple reflections in the computational domain. This is the case in the corners where two negative reflections produce a positive one, resulting in addition of the two contributions instead of the desired cancellation. The non cancellation also occurs for the multiple reflections between the wall boundary and the object inside the domain, as represented in Fig. 2-5. To overcome the corner problem, Ramahi proposed the replacement of two calculations with four, with the disposal of positive and negative reflections (i.e. of operators on the sides of the domain) represented in the right-hand part of Fig. 2-5. This widely reduces the overall reflection, but it is costly, in 2D with the four calculations, and in 3D where the method can be generalized with eight calculations.

To reduce the overall requirements, Ramahi then proposed the Concurrent complementary operator method (C-COM) [30]. The four, or eight, domains are limited to boundary regions a few cells in thickness, which are solved simultaneously with FDTD, while the interior domain is not duplicated. Each boundary region is bounded with one of the four (eight in 3D) dispositions of operators schematized in Fig. 2-5. And each region is connected to the central region through an interface, by means of the transverse derivatives on space. This permits the cancellation of the reflections from the sides

and corners of the outer domain as they enter the inner domain. However, these reflections are then reflected back by the interface towards the outer boundary where they are reflected another time towards the inner domain with the same sign (see Fig. 13 in [30]). At the end, the mechanism produces a second order reflection. If the reflection from the operator used on the boundary is R , the reflection towards the inner region is R^2 . This is a serious progress. However, in theory the same result could be achieved by just squaring the operator. The C-COM may have an advantage in the fact that it also acts on the evanescent waves, which is not the case with usual Higdon operators (but may be also the case when using the Betz-Mittra α coefficient).

To conclude, the complementary operator method has been a major achievement in ABC technology. It permits the performance of existing analytical methods, mainly the Higdon operator ABC, to be seriously boosted. It has not been adopted in numerical electromagnetics mainly because it appeared about simultaneously with the PML ABC. Otherwise, despite its drawbacks, it would have been widely used, especially in applications where a large dynamic range is needed in the computational domain. And it will be seen further in this document that the idea of complementariness of reflections also is useful to interpret and understand the reflection observed from the PML ABC.

II-6. The Matched Layer (ML) ABC

The matched layer ABC [5, 6, 7] consists in using a layer of absorbing medium placed in front of the outer boundary of the computational domain, as represented in Fig. 2-6. Many physical media do absorb the electromagnetic waves, but all produce a significant reflection from the vacuum-medium interface, because of the mismatch of their impedance with that of a vacuum. From this, physical lossy media cannot be used to realize an effective ABC.

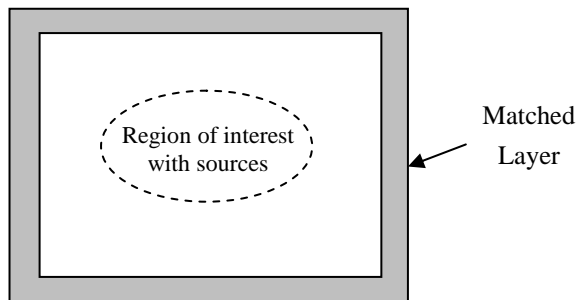


Fig. 2-6. The matched layer absorbing boundary condition surrounding a computational domain.

An approximate solution to what can be viewed as contradictory requirements has been found by using an artificial medium with a magnetic conductivity in addition to the electric conductivity [5, 6, 7]. Provided a certain relationship holds, the impedance of the medium equals that of a vacuum. The reflection from the interface is then strongly reduced. More precisely, it equals zero at normal incidence and remains small as long as the incidence is not too large.

The matched layer medium is therefore defined as a medium where the equations governing E and H fields read

$$\epsilon_0 \frac{\partial \vec{E}}{\partial t} + \sigma \vec{E} = \text{curl} \vec{H} \quad (2-62)$$

$$\mu_0 \frac{\partial \vec{H}}{\partial t} + \sigma^* \vec{H} = -\text{curl} \vec{E} \quad (2-63)$$

It can be easily found [6] that its impedance $Z = H/E$ equals that of a vacuum, provided that

$$\frac{\sigma}{\epsilon_0} = \frac{\sigma^*}{\mu_0} \quad (2-64)$$

With such a matching condition, the absorption in the medium over range x is

$$A = e^{-\frac{\sigma}{\epsilon_0 c} x} \quad (2-65)$$

and the reflection coefficients r_p and r_s of a traveling plane wave at incidence θ on the vacuum-medium interface read

$$r_p = -r_s = r = \frac{\sqrt{1 - \sin^2 \theta} / \left(1 - j \frac{\sigma}{\epsilon_0 \omega}\right)^2 - \cos \theta}{\sqrt{1 - \sin^2 \theta} / \left(1 - j \frac{\sigma}{\epsilon_0 \omega}\right)^2 + \cos \theta} \quad (2-66)$$

Formulae (2-65) and (2-66) are derived in [6], but they can also be obtained as special cases of PML media from [4] or [26]. At high frequency, when $\sigma/\epsilon_0 \omega \ll 1$, the reflection (2-66) vanishes for any incidence θ . Conversely, at low frequency, when $\sigma/\epsilon_0 \omega \gg 1$, it becomes

$$r = \frac{1 - \cos \theta}{1 + \cos \theta} \quad (2-67)$$

Unfortunately, using the medium for the absorption of outgoing waves in numerical methods corresponds to the low frequency case. This is because a sufficient attenuation must be achieved in the ML over a thickness of a few FDTD cells or a few FEM elements. That is over a thickness shorter than the wavelength λ , which is large v.s. the discretization on space in numerical methods. From the attenuation (2-65), this means that σ must be large enough in order that $\lambda \sigma/\epsilon_0 c > 1$, or equivalently, $\sigma/\epsilon_0 \omega > 2 \pi$. The reflection (2-66) from the interface of the ML used as an ABC is then, in practical situations, given by (2-67). This reflection is the same as that from a first-order analytical ABC (2-9). In addition to (2-67), there is the reflection from the outer PEC, which from (2-65) equals $\exp(-2 \sigma \delta / \epsilon_0 c)$ at normal incidence for a ML thickness δ . But it can be reduced at will by means of σ and δ . For the evanescent waves, the reflection from PML media is discussed further in this document. The discussion also applies to the ML case (especially at normal incidence where ML and PML are identical). As the PML, the ML may strongly reflect the evanescent fields.

The ML ABC has been used extensively in NEMP calculations, in France and may be also elsewhere [7]. It was implemented in the FDTD computer codes as a layer of only

three or even two cells in thickness (the computational domains were typically $< 100^3$ cells in size in the 70-80's so that the room for the ABC was limited). The conductivity σ was growing from a small value in the interface to a large enough value on the outer side, in order that the theoretical attenuation (2-65) over two ML thicknesses was about 99% (i.e. the reflection from the outer PEC was about 1%). Comparisons were later performed with the Higdon operators in this kind of applications. They showed similar performances, even with the second-order Higdon operator. In both cases the results of calculations were correct on condition that the ABC is placed at a sufficient distance from the scattering objects. This is because both the operators and the ML strongly reflect the evanescent waves. Some comparisons of the ML ABC with the Higdon and Mur ABCs can be found in papers [4, 31, 33].

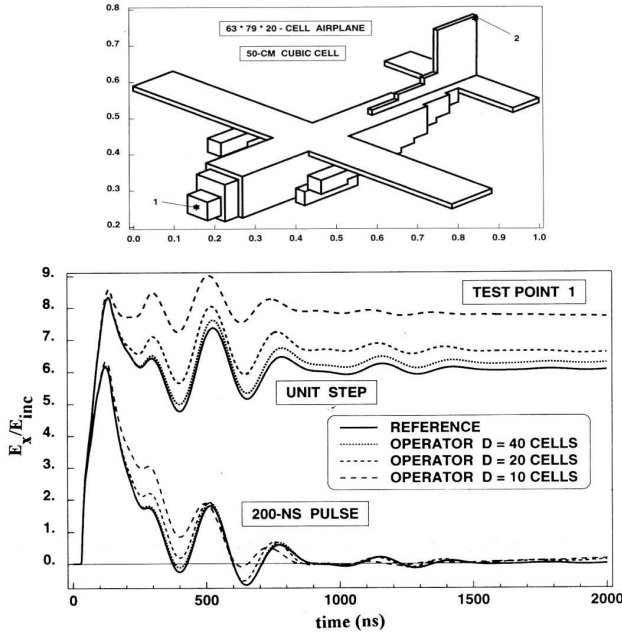


Fig. 2-7. E field produced on the PEC surface of a 64-79-20-cell aircraft structure with a 2-order Higdon ABC placed several distances from the aircraft, for a double-exponential 200-ns pulse and for a unit-step pulse. For $D = 40$ cells the aircraft-operator separation is about half the span of the aircraft (79 cells).

II-7. Summary on the analytical ABCs

There have been numerous absorbing boundary conditions introduced in the 70's and 80's. They are effective for the absorption of traveling waves, but little effort was paid to the absorption of evanescent waves, so that most ABCs reflect in totality the evanescent fields, except the complementary operators and the Betz-Mittra ABC. In many applications the consequence was the need of placing the ABC some distance away from the region of interest, in order that the evanescent fields decrease naturally to a sufficiently small level. This is illustrated with the example in Fig. 2-7 from [31] where the field on a airplane structure has been computed for two incident plane waves, with the Higdon second order ABC placed several distances (10, 20, 40 FDTD cells) from the object (from the parallelepiped that just fits the airplane). A

distance larger than half the size of the object is needed in order that the low frequency evanescent fields, reflected in totality by the ABC, decrease naturally to a negligible level. The same observation can be seen also in [3] with the radiating boundary ABC.

III. THE PERFECTLY MATCHED LAYER

The perfectly matched layer ABC was published in 1994 [4] as an ABC for the solution of the Maxwell equations with the FDTD method. It was rapidly extended to other numerical techniques, and to other media than vacuum. In the following, section 3-1 recalls how the PML was elaborated in the simple two dimensional case. Section 3-2 briefly reviews the different forms of 3D PMLs which are well known and well documented in the literature and in textbooks. The other sections discuss with more details the critical question of the absorption and reflection of the evanescent waves by PMLs, especially in the discrete space of the finite methods.

III-1. The PML in two dimensions

The matched layer was simple to implement, with no problem of stability, and was almost as effective as high-order analytical ABCs. At normal incidence it was perfect, so that it appeared that a challenging question was how to reduce its reflection at oblique incidence. This was achieved by observing that some modifications of the equations permit the free propagation of waves in the direction parallel to the vacuum-medium interface, i.e. at grazing incidence. Let us consider the 2D z -invariant case where the field components are E_x, E_y, H_z . The ML equations read

$$\epsilon_0 \frac{\partial E_x}{\partial t} + \sigma E_x = \frac{\partial H_z}{\partial y} \quad (3-1a)$$

$$\epsilon_0 \frac{\partial E_y}{\partial t} + \sigma E_y = -\frac{\partial H_z}{\partial x} \quad (3-1b)$$

$$\mu_0 \frac{\partial H_z}{\partial t} + \sigma^* H_z = \frac{\partial E_x}{\partial y} - \frac{\partial E_y}{\partial x} \quad (3-1c)$$

where σ and σ^* satisfy (2-64). Let us now consider the following modified equations

$$\epsilon_0 \frac{\partial E_x}{\partial t} = \frac{\partial(H_{zx} + H_{zy})}{\partial y} \quad (3-2a)$$

$$\epsilon_0 \frac{\partial E_y}{\partial t} + \sigma E_y = -\frac{\partial(H_{zx} + H_{zy})}{\partial x} \quad (3-2b)$$

$$\mu_0 \frac{\partial H_{zx}}{\partial t} + \sigma^* H_{zx} = -\frac{\partial E_y}{\partial x} \quad (3-2c)$$

$$\mu_0 \frac{\partial H_{zy}}{\partial t} = \frac{\partial E_x}{\partial y} \quad (3-2d)$$

where the H_z component is split into two subcomponents H_{zx} and H_{zy} , and where equation (3-1c) is split into (3-2c) and (3-2d). The medium (3-2) is represented in Fig. 3-1 with two plane waves propagating in the directions normal to the interface and parallel to the interface, respectively. Since the incident wave A is invariant in y direction, its propagation in

the medium is only governed by (3-2b) and (3-2c). For wave A, the medium is a matched medium, with zero reflection from the interface. Consider now plane wave B, assumed as set as an initial condition invariant in x direction, i.e. with derivatives in x direction equal to zero in both media. The propagation is governed by (3-2a) and (3-2d). The other two equations play no role. For wave B, the medium is viewed as a vacuum, in other words, at grazing incidence the medium (3-2) produces no reflection. Then, $r = 0$ at both normal and grazing incidences.

Derivations in [4] show that $r(\theta) = 0$ at any incidence θ . The medium (3-2) is perfectly matched to a vacuum in the sense that it produces no reflection of incident waves.

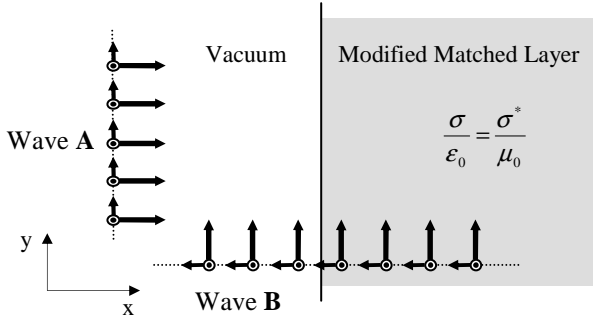


Fig. 3-1. Plane waves at normal and grazing incidences with respect to the interface between a vacuum and the modified matched medium (3-2).

More generally, the 2D (TE case) PML medium is defined as

$$\epsilon_0 \frac{\partial E_x}{\partial t} + \sigma_y E_x = \frac{\partial(H_{zx} + H_{zy})}{\partial y} \quad (3-3a)$$

$$\epsilon_0 \frac{\partial E_y}{\partial t} + \sigma_x E_y = -\frac{\partial(H_{zx} + H_{zy})}{\partial x} \quad (3-3b)$$

$$\mu_0 \frac{\partial H_{zx}}{\partial t} + \sigma_x^* H_{zx} = -\frac{\partial E_y}{\partial x} \quad (3-3c)$$

$$\mu_0 \frac{\partial H_{zy}}{\partial t} + \sigma_y^* H_{zy} = \frac{\partial E_x}{\partial y} \quad (3-3d)$$

where (σ_x, σ_x^*) and (σ_y, σ_y^*) satisfy the matching condition (2-64). Equations (3-2) are just the special case of (3-3) with $\sigma_y = \sigma_y^* = 0$. Similarly, an interface perpendicular to y direction produces no reflection provided that $\sigma_x = \sigma_x^* = 0$. Combination of the two special cases permits an ABC to be constructed on the outer boundary of a 2D computational domain, as represented in Fig. 3-2. In the corners, both (σ_x, σ_x^*) and (σ_y, σ_y^*) are present, in such a way that the transverse conductivities are equal at all the small corner interfaces. This permits the reflection from these interfaces to be null [4].

An important interpretation of the PML medium (3-3) comes by rewriting it in frequency domain, that is by replacing the derivatives on time with $j\omega$. Then, (3-3c) and (3-3d) can be added so that set (3-3) reduces to three equations:

$$j\omega\epsilon_0 E_x = \frac{1}{s_y} \frac{\partial H_z}{\partial y} \quad (3-4a)$$

$$j\omega\epsilon_0 E_y = -\frac{1}{s_x} \frac{\partial H_z}{\partial x} \quad (3-4b)$$

$$j\omega\mu_0 H_z = -\frac{1}{s_x^*} \frac{\partial E_y}{\partial x} + \frac{1}{s_y^*} \frac{\partial E_x}{\partial y} \quad (3-4c)$$

where

$$s_u = 1 + \frac{\sigma_u}{j\omega\epsilon_0}; \quad s_u^* = 1 + \frac{\sigma_u^*}{j\omega\epsilon_0} \quad (u=x, y) \quad (3-4d)$$

Equations (3-4) are identical to the Maxwell equations in a vacuum. They just differ with the coefficients s_x, s_x^* and s_y, s_y^* in front of the derivatives in x and y directions, respectively. The PML can be viewed as a stretch of coordinates by the

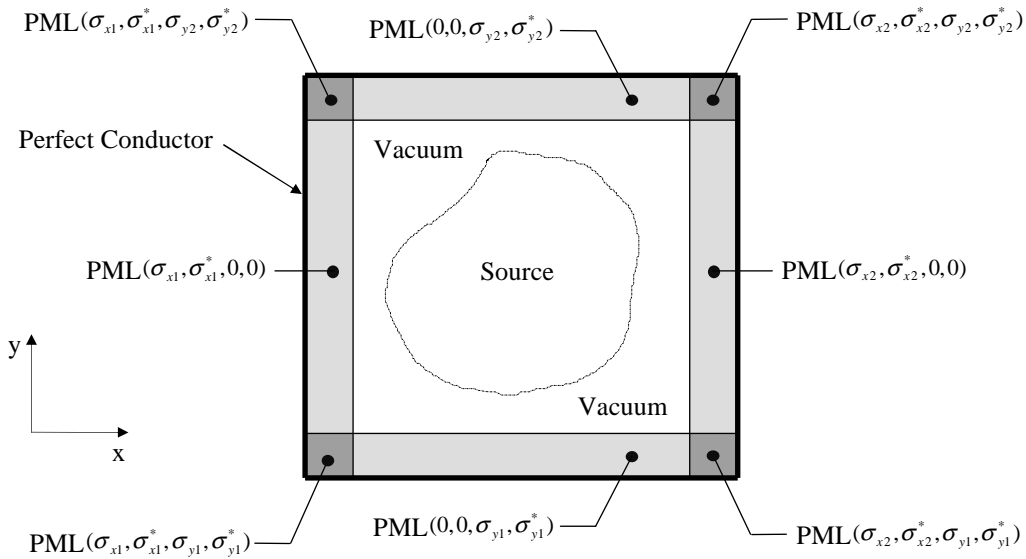


Fig. 3-2. The 2D PML ABC composed of PML media ensuring no reflection at all the interfaces.

complex factors s_u and s_u^* which are equal when the matching condition (2-64) holds. For zero reflection at an interface, the medium is only stretched in the direction perpendicular to the interface, that is x with (3-2), and left unchanged in the other direction. This is the fundamental difference with the matched medium (2-62) which can also be viewed as a stretched medium, but in all the directions of space. The interpretation of the PML in terms of stretched coordinates is due to Chew and Weddon [32]. It is essential in view of extending the PML to other media than vacuum.

Using (3-3), the equation of dispersion in the PML can be easily derived by inserting a waveform like (2-4)

$$\frac{\omega^2}{c^2} = \frac{k_x^2}{s_x s_x^*} + \frac{k_y^2}{s_y s_y^*} \quad (3-5)$$

It is satisfied by the following wavenumbers

$$k_x = \frac{\omega}{c} \sqrt{s_x s_x^*} \cos \theta \quad (3-6a)$$

$$k_y = \frac{\omega}{c} \sqrt{s_y s_y^*} \sin \theta \quad (3-6b)$$

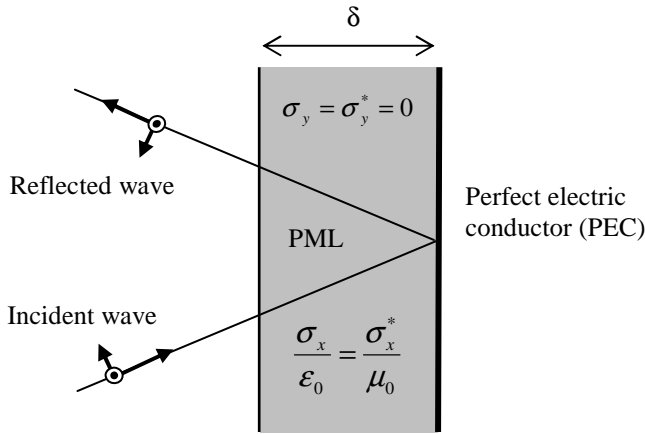


Fig. 3-3. The reflection of a plane wave from the wall PML.

In medium (3-3) only stretched in x direction ($s_y = s_y^* = 1$) the wavenumber k_y is the same as in a vacuum. From this, the equation $k_{y1} = k_{y2}$ that holds at the vacuum-PML interface implies that the angle of propagation of an incident wave is left unchanged when it penetrates into the PML (in other words, the Snell law reads $\theta_1 = \theta_2$ at the vacuum-PML interface). Using then k_x (3-6a) into (3-3) shows that the medium remains an absorbing medium. More precisely, in the PML where $\sigma_y = \sigma_y^* = 0$ and (σ_x, σ_x^*) satisfy (6-24), the field E (or H) at distance x from the vacuum-PML interface can be written as

$$E_{PML} = E_{vacuum} e^{-\frac{\sigma_x \cos \theta}{\epsilon_0 c} x} \quad (3-7)$$

which means that the waveform in the PML is the same as in a vacuum, with just in addition the attenuation by an exponential factor. We notice the attenuation depends on the angle θ . At normal incidence it equals the attenuation of the matched medium (2-62). It vanishes at grazing incidence, which is not a drawback for using the medium as an ABC. From (3-7), the reflection produced by the side PMLs (also known as the wall

PMLs) of thickness δ (Fig. 3-3) reads, in the case where the conductivity varies with x :

$$R(\theta) = e^{-2 \frac{\cos \theta}{\epsilon_0 c} \int_0^\delta \sigma_x(x) dx} \quad (3-8)$$

In principle, $R(\theta)$ can be chosen as small as needed, by increasing σ_x or δ , or both.

III-2. The PML in three dimensions and for any inner media

The above 2D PML can be extended in a trivial manner to 3D, by splitting the six components of the field into twelve subcomponents, and by splitting the six components of the Maxwell equations into twelve sub-equations [33]. This 3D counterpart of the 2D case (3-3) is known as the split PML where there are then twelve quantities (the sub-components) to be advanced in time (only ten in the wall PMLs). Another method [32] consists in generalizing (3-4) to 3D, that is stretching the coordinates in the Maxwell equations by coefficients like (3-4d). From this, other time domain equations can be derived, namely the convolutional PML (CPML), and the near PML (NPML). In the CPML introduced in [36] there are only the six components of the field, but twelve additional quantities (four in wall PMLs) must be computed and advanced in time by means of auxiliary equations. The NPML is an approximation to the PML which is identical to a PML only when the conductivity is uniform in the medium [37], but it also produces no reflection even when the conductivity varies [38, 39]. It also involves twelve additional quantities governed by twelve auxiliary equations.

Another absorbing medium which produces no reflection at the interface with the inner medium has been proposed [34, 35]. It is known as the uniaxial PML. There the fields E and H are stretched with the coefficients (3-4d), in place of the coordinates. This also results in zero reflection [34]. Its time domain equations are those of an anisotropic medium with six additional quantities (two in wall PMLs) and six auxiliary equations [35]. This medium can be used easily with the finite-element method.

The PML medium can be used as an ABC on the outer boundary of a computational domain, by extending the 2D case in Fig. 3-2. By an adequate choice of the conductivities [26, 33] there is no reflection at all the interfaces in the problem space, i.e. at the vacuum-PML interfaces as well as at the inner interfaces between the different PMLs in the corners and edges, where transverse conductivities always are identical on the two sides of the interfaces.

The PML can be extended to any media by applying the stretched mesh method (p. 38-42 in [26]), especially to lossy media, anisotropic media, or non homogeneous media. And more recently, to metamaterial media.

Each time domain PML has its own advantages and drawbacks, in terms of needed storage, computational time, and easiness to implement with complicated media. A comparison of the computational requirements can be found in (p. 68, [26]). From the works reported in the literature, it seems that the most popular implementation in the FDTD method is the CPML which can be more easily extended to any media than the split PML (this is also true for the NPML). For detailed descriptions of the different PML media and of their

time domain implementations in the FDTD method, the reader is referred to the existing textbooks [16], [17], and [26]. The PML ABC can also be used with such frequency domain methods as the parabolic equation method [61] and the finite element method where its most used version is the uniaxial PML [34].

III-3. The evanescent waves in the PML

In the above and in most papers in the literature, especially in [4, 32], only traveling waves absorbed with the coefficient in (3-7) have been addressed. They correspond to the wavenumbers (3-6). However, it can be easily verified that the following wavenumbers are also solutions of the 2D equation of dispersion (3-5):

$$k_x = \frac{\omega}{c} \sqrt{s_x s_x^*} (\cosh \chi \cos \theta + j \sinh \chi \sin \theta) \quad (3-9a)$$

$$k_y = \frac{\omega}{c} \sqrt{s_y s_y^*} (\cosh \chi \sin \theta - j \sinh \chi \cos \theta) \quad (3-9b)$$

where χ and θ are free parameters. They just differ from the wavenumbers in a vacuum (2-10)-(2-11) with the square root of the stretching factors. And when $\chi=0$ they reduce to those of a traveling wave propagating in direction θ (3-6). Inserting (3-9) into the waveform (2-4), and using the change of coordinates defined in appendix A, the following waveform is obtained:

$$E = E_0 e^{j\omega \left(t - \frac{\cosh \chi X - \frac{\sigma_x}{\epsilon_0 c} \sinh \chi \sin \theta x}{c} \right)} e^{-\frac{\omega}{c} \sinh \chi Y} e^{-\frac{\sigma_x}{\epsilon_0 c} \cosh \chi \cos \theta x} \quad (3-10)$$

The two terms depending on X and Y are nothing but the waveform of an evanescent wave in a vacuum (see appendix A), whose phase propagates in direction X forming the angle θ with x , and whose magnitude decreases in direction Y perpendicular to X . The two additional exponentials are a phase term and an absorbing term. This shows that in a PML the evanescent waves can be written as

$$|E_{PML}| = |E_{vacuum}| e^{-\frac{\sigma_x \cosh \chi \cos \theta x}{\epsilon_0 c}} \quad (3-11)$$

Since $\cosh \chi > 1$, the absorption of evanescent waves in the PML is larger than that of traveling waves (3-7).

It was derived in [40] that in continuous spaces the evanescent waves are not reflected from a vacuum-PML interface. As the traveling waves they can penetrate in totality into the PML. The angle of the propagation of the phase θ is left unchanged through the interface, as well as the evanescence coefficient χ . In theory, the PML is then perfectly matched to the evanescent waves. However, in discrete spaces we can expect some spurious effects when the PML conductivity has been chosen in order that the absorption (3-7) is sufficient to absorb the traveling waves. Then, the absorption of strongly evanescent waves, when $\cosh \chi \gg 1$, may be quite high. In consequence, it may correspond to a total absorption over a distance shorter than one cell with the FDTD method or one element with the FEM, as represented in Fig. 3-4. From (3-11), this occurs when:

$$\cosh \chi \gg \frac{\epsilon_0 c}{\sigma_x \Delta x} \quad (3-12)$$

It is obvious that the FDTD mesh cannot properly sample such waves that decrease too rapidly. From this, a significant reflection of strongly evanescent wave can be expected from the vacuum-PML interface. This has been confirmed by numerical experiments and by the theory of the evanescent waves in the discrete FDTD method [40], as discussed with details in the next section. We can also notice that when (3-12) holds, the phase term in (3-10) produces rapid variations of the phase with respect with the cell Δx . This cannot be sampled by the mesh as well, and also may contribute to the spurious reflection.

III-4. The numerical reflection from the PML

In theory, any desired small reflection (3-8) can be achieved by using a large enough product $\sigma_x \delta$. More specifically, any small reflection can be achieved with an arbitrary short thickness δ , provided that σ_x is large enough. This means that the PML could be one cell in thickness with the FDTD method (one element with the FEM). In practice, as soon as the early experiments [4], it appeared that the PML can achieve far better performance than previous ABCs, but on condition that it is some FDTD cells in thickness. There exists a spurious reflection, not predicted by (3-8), which is due to the discretization of the medium. This reflection decreases when the thickness grows and when σ_x grows from a small value in the interface to a larger value in the outer cell of the PML. This is in accordance with the known fact that at an interface between two physical media, as air and a dielectric, a spurious reflection is added to the physical reflection when using discrete methods. The same occurs with the air-PML interface.

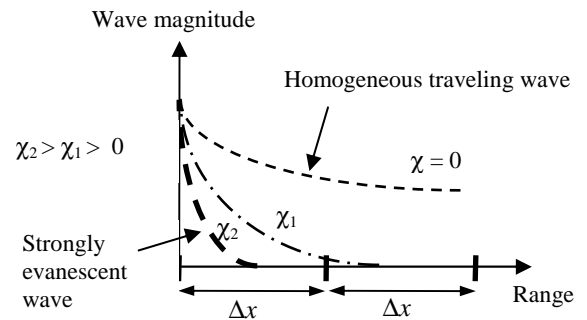


Fig. 3-4. Theoretical decrease of evanescent waves in the FDTD grid for several values of the parameter χ .

In the following, the discussion of the numerical reflection is limited to the FDTD method. The reflection with other discrete methods (FEM, TLM, others), would not be very different because it is mainly produced by the too rapid decrease of the field with respect with the space sampling in the PML. More specifically, using the same sampling (the same cell or element), the numerical reflections produced by different methods are similar, as it is illustrated with the FDTD-TLM comparison reproduced in [26].

We must now distinguish two cases, the pure traveling waves, and the evanescent waves, which are fundamentally

different from the point of view of the numerical reflection produced by a PML.

The numerical reflection of traveling waves

Numerous experiments were reported in [4] and elsewhere, but the first theoretical study of the spurious reflection of traveling waves was reported in [41] for the air-PML interface. More generally, for a PML where the conductivity grows from one cell to the next, the reflections from all the inner interfaces must be taken into account to obtain the overall reflection. To predict this overall reflection, the formulae (a tri-diagonal system) derived in [40] can be used in the special case of traveling waves ($\cosh\chi=1$).

In general, the numerical reflection of traveling waves is relatively small. It is not a challenging question. It depends on the profile of conductivity in the medium, and satisfactory results can be obtained with polynomial profiles (power 2 or 3 usually). Fig. 3-5 shows an example. With a parabolic profile and a PML only four cells in thickness, reflections as low as -80 dB can be achieved at normal incidence. Notice that when the theoretical reflection $R(0)$ decreases, the numerical reflection (difference between theory and FDTD in the figure) grows. It is rather counterproductive to use a too small $R(0)$. For given PML thickness and profile of conductivity, there is an optimum $R(0)$ where the actual FDTD reflection is minimum. Reducing further the reflection requires increasing the PML thickness. The experiments in [4] demonstrate the evolution of the actual reflection with some parameters (thickness, profile, $R(0)$). It is easy to predict this reflection using the formula in [40], which is also available in the form of software [42].

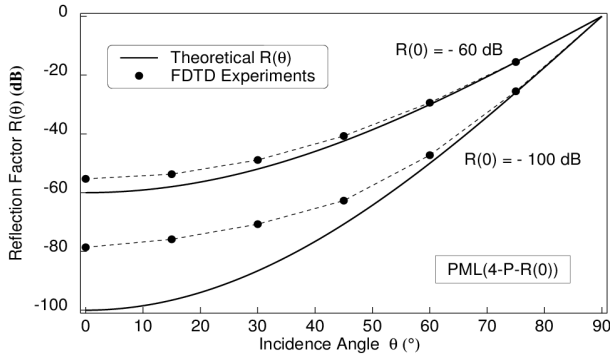


Fig. 3-5. Comparison of the theoretical reflection $R(\theta)$ with the reflection observed in FDTD experiments with plane waves.

The numerical reflection of evanescent waves

The reflection of evanescent waves has been, and remains in part, a challenging question. In the initial experiments [4], it appeared that in such problems as wave-structure interactions, strong low frequency spurious fields are present, as with analytical ABCs. However, by using a thick enough PML, the reflection could be reduced and the PML placed in the close vicinity of the scattering objects. Such an achievement was not possible with Mur or Higdon ABCs, with which the ABCs had to be placed far from the objects, out of the evanescent region. This kind of problems was initially analyzed empirically, and guidelines for choosing the PML were reported in [43, 44].

Understanding the reason of the low frequency spurious reflection from PMLs began with the pioneering work of De Merloose and Stucky [45] who showed that the actual reflection from FDTD PMLs can be predicted theoretically for waves evanescent in the direction perpendicular to the PML interface (at the end of a waveguide). This reflection can be large and even total, because of the rapid variation of the phase of evanescent waves in the PML, upon characteristic distances far shorter than the FDTD cell size. This case corresponds to $\theta = \pi/2$ in wavenumbers (3-9).

Following the way open by [45], the theory of general evanescent waves in PML media was derived, both in continuous space and in the discretized space of the FDTD method [46, 40]. The theory permits the spurious reflection of low frequency observed in experiments to be interpreted and well understood. As discussed in the previous section, the evanescent waves penetrate without reflection in the continuous PML. This is no longer true in the discrete FDTD space. For a PML with uniform conductivity the reflection from the interface is given by an analytical formula (23 in [40] or 5-45 in [26]). In the case of strongly evanescent waves, i.e. when $\cosh\chi$ satisfies (3-12), the formula reduces to:

$$R_{\infty} = \frac{j \frac{f_c}{f}}{1 - j \frac{f_c}{f}} \quad (3-13)$$

with

$$f_c = \frac{\sigma_{x0}}{2\pi\epsilon_0} \quad (3-14)$$

where σ_{x0} is the conductivity in the interface which may be different from the uniform conductivity σ_x set at the other FDTD nodes of the PML (as $\sigma_{x0} = \sigma_x/2$).

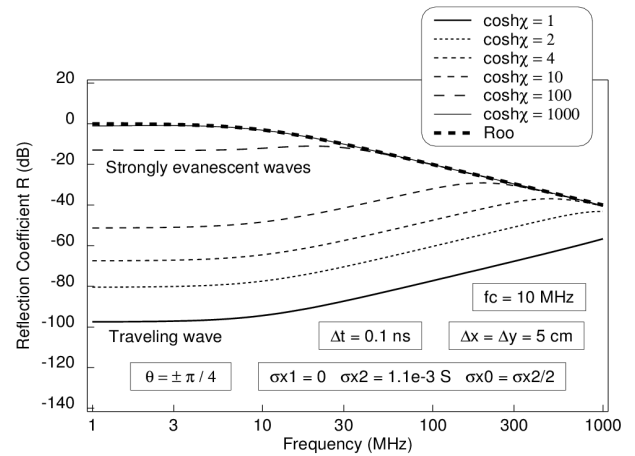


Fig. 3-6. FDTD reflection from the interface between a vacuum and a uniform infinite PML, from traveling wave ($\cosh\chi = 1$) to strongly evanescent waves ($\cosh\chi = 1000$).

Formula (3-13) shows that when (3-12) holds the reflection from the interface decreases at high frequency ($f \gg f_c$), but it is total ($R_{\infty} = -1$) at low frequency ($f \ll f_c$). The total reflection below f_c was expected since when (2-12) holds the evanescent waves are absorbed, in theory, over less than one FDTD cell, which cannot be achieved by the FDTD method. Fig. 3-6, from

[40] shows the reflection coefficient computed with the formula in [40, 26], at the incident angle $\theta = \pi/4$, which means that the evanescence is also $\pi/4$ from the interface. The PML conductivity in the interface is such that $f_c = 10$ MHz. The reflection is plotted for $\cosh\chi$ varying from 1 (traveling wave) to 1000. For the traveling wave the reflection grows as the frequency is approaching the cut-off of the FDTD mesh. It is very small (-100 dB) at low frequency. Conversely, for the strongly evanescent waves the reflection grows as the frequency decreases and it is total below f_c , in accordance with (3-13). Notice that the condition (3-12) for the validity of (3-13) is $\cosh\chi \gg 40$ in the conditions of Fig. 3-6. This is well verified.

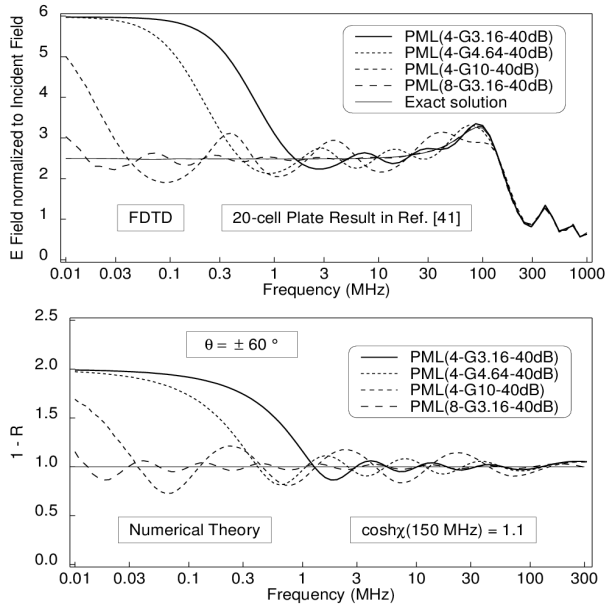


Fig. 3-7. Comparison of the spurious FDTD field observed on a 2D thin plate with the factor $1-R$, where R is the theoretical reflection of evanescent waves by a PML with conductivity growing geometrically (see more details in [40]). The oscillations of the spurious field illustrate the reflection by the inner interfaces of the PML, which are alternatively of electric and magnetic kinds. The two parts should be compared only below 30 MHz (above, the traveling waves are predominant, they are absent in the theoretical lower part).

In the case of a PML with σ_x growing from a small value in the interface, the situation is more complex. The reflection is given by a simple tri-diagonal system [40, 26, 42]. For $f < f_c$ and strongly evanescent waves (3-12), the reflection also reduces to (3-13). But every inner interface has its own frequency f_c proportional to its conductivity. So that frequencies that penetrate through the vacuum-PML interface may be reflected from the inner interfaces. Since in the FDTD grid there are electric and magnetic interfaces (interfaces where the tangential fields are either E or H , separated with $\Delta x/2$), the internal reflections are alternatively of opposite signs. From this, the numerical reflection of strongly evanescent waves oscillates as the frequency grows. This is well predicted by the theoretical formula in [40, 26], and very well verified in experiments. An experiment reported in [40] is reproduced in Fig. 3-7. The upper part shows the E field on the surface of a thin PEC plate stricken by an incident wave, with

several PMLs placed close to the plate, two FDTD cells from it. In each case, the low frequency plateau is strongly erroneous, corresponding to the reflection by the vacuum-PML interface for $f < f_c$. At higher frequencies, the oscillations are produced by the reflections from the successive inner interfaces. The lower part shows that the general shape of the reflection of the evanescent waves can be very well reconstructed by means of the formula in [40, 26]. In fact, the PML works as a set of complementary reflectors, in the sense of the complementary operators of Ramahi (see section 2-4). If the ratio of frequencies f_c of the inner interfaces is not too large, each frequency experiences several partial reflections of opposite signs from several interfaces. The overall reflection of this frequency is then smaller than total reflection, and the closer the f_c 's, the smaller the overall reflection.

In summary, the evanescent waves are reflected by the PML in such discretized spaces as the FDTD space. However, and conversely to most analytical ABCs, it is possible to reduce the reflection, by increasing the PML thickness and by using a conductivity that grows in the PML. Two conditions must hold for the reflection of evanescent waves is small enough:

1/ the conductivity σ_{x0} in the vacuum-PML interface must be small enough in order that the frequency f_c (3-14) is smaller than the lowest frequency of interest of the problem.

2/ the conductivity must grow at a small rate from one FDTD node to the next, in order to reduce the reflection from the inner interfaces, or, in other words, to maximize the Ramahi effect.

Optimum PMLs satisfying 1/ and 2/ for solving wave-structure interaction problems were elaborated [43, 44]. However, they cannot be applied to any problems because they depend on the general form of the evanescent fields and on the desired accuracy. In practice, it seems that is many, not to say most, cases reported in the literature, the PML is chosen mainly empirically, by performing several tests to find the minimum thickness needed for solving the problem under interest. It should be noticed that the choice of the PML (split PML, uniaxial PML, CPML, NPML) has little effect on the FDTD reflection of both traveling and evanescent waves. This was demonstrated both theoretically and by experiments in [47] and [39].

The next section is devoted to the complex frequency shifted PML (CFS-PML), which permits the reflection of evanescent waves from PMLs to be dramatically reduced in many physical problems. This is obtained by means of a modified stretching factor.

III-5. The complex frequency shifted PML

The CFS-PML was introduced in 1996 by Kuzuoglu and Mittra [48] with the intention of rendering the PML medium causal. To this end, they replaced the stretching factors (3-4d) with the following, for the stretch in x direction

$$s_x = 1 + \frac{\sigma_x}{\alpha_x + j\omega\epsilon_0} \quad (3-15)$$

where α_x is a real positive parameter. The stretching factor remains finite as frequency vanishes which render the medium causal [48]. Another interest of this modified stretched factor was found later [36, 47]. It permits the reflection of evanescent

waves from PMLs to be dramatically reduced in many applications of finite methods.

With (3-15), it is evident that frequency

$$f_\alpha = \frac{\alpha_x}{2\pi\epsilon_0} \quad (3-16)$$

is a critical parameter. For $f \gg f_\alpha$, the CFS-PML is a normal PML since then α_x is negligible in (3-15). Conversely, when $f \ll f_\alpha$ the complex term is negligible and the CFS-PML is just a real stretch of coordinates. It does not absorb the waves.

Using wavenumbers (3-9) and coefficient (3-15) into (2-4), the waveform can be obtained in the CFS-PML [47]. As expected, for $f \gg f_\alpha$, it reduces to the waveform in a normal PML, so that (3-11) remains valid. Conversely, if $f \ll f_\alpha$ the waveform is different [47, 26]. Its magnitude decreases in the PML according to

$$|E_{PML}| = |E_{vacuum}| e^{\frac{f}{f_\alpha} \frac{\sigma_x \sinh \chi \sin \theta}{\epsilon_0 c} x} \quad (3-17)$$

where θ is negative when the evanescence is towards the PML (appendix A). For low frequency ($f \ll f_\alpha$) and strongly evanescent waves where $\sinh \chi \sim \cosh \chi \gg 1$, it is evident that the attenuation coefficient of (3-17) is by far smaller than that of (3-11). This may result in a reasonable attenuation of evanescent waves, and then a dramatic reduction of their reflection from the discrete vacuum-PML interface.

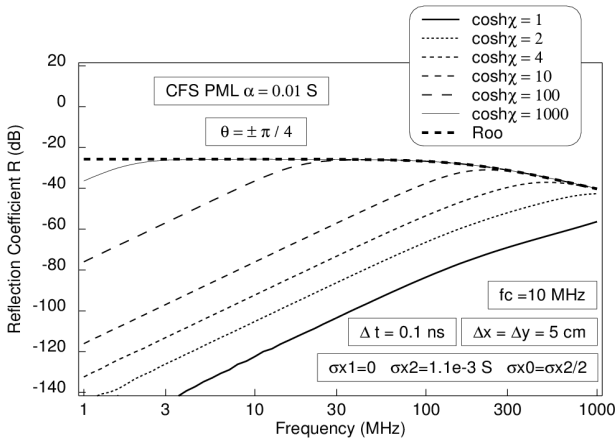


Fig. 3-8. FDTD reflection from the interface between a vacuum and a uniform infinite CFS-PML, from traveling wave ($\cosh \chi = 1$) to strongly evanescent waves ($\cosh \chi = 1000$).

As with the standard PML, the FDTD reflection from a CFS-PML with uniform conductivity is given by a formula, and from a CFS-PML with growing conductivity by a tri-diagonal system [47, 26]. In both cases, for strongly evanescent waves (3-12) the reflection from the vacuum-PML interface tends to the following formula, in place of (3-13):

$$R_\infty = \frac{j \frac{f_{c\alpha}}{f} \sigma_{x0}}{1 - j \frac{f_{c\alpha}}{f} \alpha_{x0} + \sigma_{x0}} \quad (3-18)$$

with

$$f_{c\alpha} = \frac{\alpha_{x0} + \sigma_{x0}}{2\pi\epsilon_0} \quad (3-19)$$

where α_{x0} and σ_{x0} are α_x and σ_x in the FDTD interface. The reflection (3-18) tends to $\sigma_{x0}/(\alpha_{x0} + \sigma_{x0})$ at low frequency in place of the total reflection of the standard PML (3-13). This is illustrated by Fig. 3-8 which is the counterpart of Fig. 3-6. With $\alpha_{x0} = 0.01$ S and the conductivity in the figure, the reflection of evanescent waves is about -25 dB, whatever may be the evanescence parameter $\cosh \chi$. Other results illustrating the FDTD reflection by the CFS-PML can be found in [47].

The effectiveness of the CFS-PML for reducing the reflection of evanescent waves is demonstrated in the following, for a waveguide problem and for the interaction of an incident wave with an object. Let us first consider a parallel plate waveguide with separation a between the plates. The mode n is evanescent below its cutoff which reads $\omega_c = n\pi c/a$, and its $\sinh \chi$ parameter is given by

$$\sinh \chi = \pm \sqrt{\frac{\omega_{cutoff}^2}{\omega^2} - 1} \quad (3-20)$$

Thus, far below the cutoff the following holds

$$\omega \sinh \chi = \pm \frac{n\pi c}{a} \quad (3-21)$$

From this the attenuation in (3-17) does not depend on frequency far below the cutoff. By an adequate choice of the free parameter f_α , the attenuation of the evanescent waves (3-17) and that of the traveling waves (3-7) can be set equal. Assuming that $\sin \theta \sim 1$, this is realized with the following f_α :

$$f_\alpha = \frac{nc}{2a} \quad (3-22)$$

which yields, using (3-16):

$$\alpha_x = n \frac{\pi c \epsilon_0}{a} \quad (3-23)$$

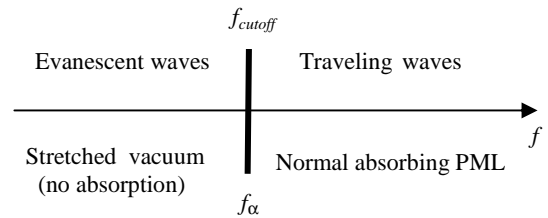


Fig. 3-9. Coincidence of the transition frequency of the CFS-PML with the cutoff frequency of the parallel-plate waveguide.

We can notice that $f_\alpha = f_{cutoff}$. The situation is then as represented in Fig. 3-9. For the traveling waves, above the cutoff, the CFS-PML is a standard absorbing PML. Conversely, for the evanescent waves, below the cutoff, the CFS-PML is just a real stretch of coordinates, with no absorption. There the evanescent waves decrease in a natural manner over the stretched space, resulting in an apparent absorption identical to that of the traveling waves, and in consequence with little numerical reflection from the vacuum-PML interface. Numerical experiments with this waveguide problem are reported in [49]. They show that the CFS-PML

can achieve reflections of evanescent frequencies below -80 dB with a CFS-PML only 6 FDTD cells in thickness.

Another case where the CFS-PML permits the reflection of low frequency to be reduced is when an incident wave strikes a scattering structure. In that case, a relationship like (3-21) also holds, more precisely (see appendix B):

$$\omega \sinh \chi = p \frac{c}{w} \quad (3-24)$$

where w is the largest size of the structure and p is a parameter of the order of unity. By assuming that $p = 1$, the attenuations of traveling (3-7) and evanescent (3-17) waves are equal provided that

$$\alpha_x = \frac{c \epsilon_0}{w} \quad (3-25)$$

This corresponds to $f_\alpha = f_0/\pi$ where $f_0 = c/2w$ is the fundamental resonance of the structure. The situation is then the same as in Fig. 3-9. For the high frequencies above f_0 , which are traveling frequencies, the CFS-PML is a standard absorbing PML. And for the low frequencies below f_0 , which are evanescent, the CFS-PML is just a real stretch of coordinates that permits them to decrease in a natural manner. The FDTD reflection from the vacuum-PML interface, and from the inner interfaces of the PML, is then quite small for all the frequencies.

The CFS-PML for wave-structure interactions has been well studied and optimized [50, 26, 27]. It permits low reflections to be achieved with CFS-PMLs only 3-5 cells in thickness, with a short separation of two FDTD cells between the PML and the structure of interest. Numerical experiments and the recommended parameters of the CFS-PML for this kind of applications are provided with details in [27]. Fig. 3-10 shows an example, with the same aircraft structure as in Fig. 2-7, but re-gridded with smaller FDTD cells (6.25 cm in place of 50 cm). The results are superimposed on the reference solution with a CFS-PML only 3-4 cells in thickness placed two cells from the structure. Achieving such a performance with the second order Higdon operator would require a huge amount of vacuum around the aircraft, as demonstrated by Fig. 2-7 where the results are not perfect even with a separation of the order of half the size of the object (this is the physical separation between the object and the Higdon operator which permits the evanescent wave to decrease, computing the equivalent of result D = 40 cells in Fig. 2-7 would require D = 320 cells with the re-gridded aircraft).

From the above, the CFS-PML permits an effective absorption of evanescent waves with little reflection, by choosing the parameter α_x in such a way that the attenuation of the traveling and evanescent waves are equal. However, a weakness of the method is that the optimum α_x may not be unique. With the waveguide problem, the optimum α_x depends on the mode (3-23). Similarly, with the scattering problem, α_x depends on the parameter p . The problem has been overcome in the optimum CFS-PML [27, 26] by using a parameter α_x that varies in the PML, from a value larger than (3-25) in the interface to a value smaller than (3-25) at the outer end. This results in a satisfactory optimum CFS-PML for the kind of problems addressed in [27], mainly electromagnetic compatibility (EMC) problems. A similar strategy could also be used with waveguide problems where several modes are present, at least when the cutoff frequencies of the modes are

not too different. This has never been tested. Another weakness of the CFS-PML optimisation is that the Physics of the problem must be known a priori, that is the relationship between frequency and the $\sinh \chi$ parameter of the evanescent waves must be roughly known. This may be difficult or not possible in some problems. In the literature, the CFS-PML is widely used. However, in most cases the choice of α_x is done without reasoning and without convincing argumentation. Probably empirically by performing some experiments with the problem under investigation to find which value gives the best results.

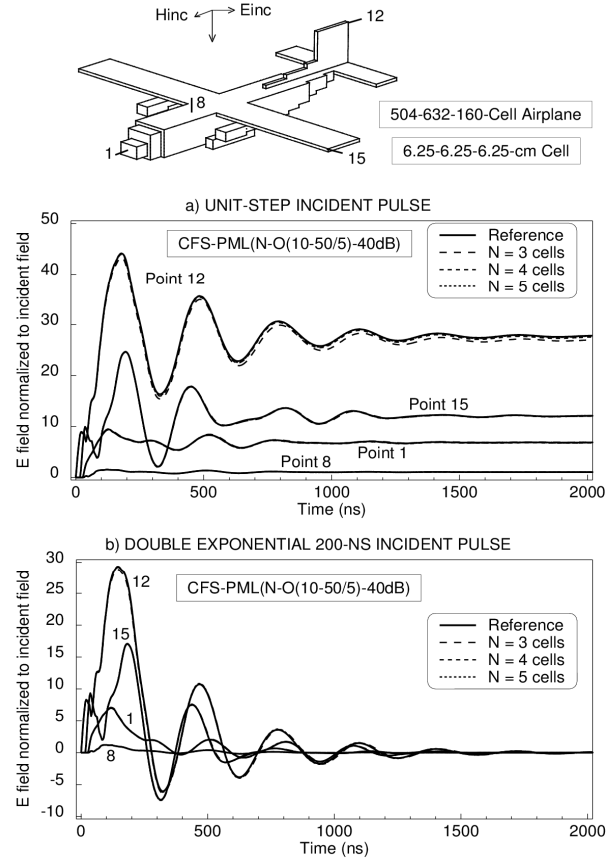


Fig. 3-10. Electric field on the surface of a 504-632-160-cell airplane with 3-, 4-, 5-cell CFS-PMLs, for a unit-step and a 200-ns double exponential waves. From the interface to the outer end, the conductivity grows by a factor of 10 and the parameter α_x decreases from 50 to 1/5 of value (3-25). The CFS-PML is two cells from the structures (from the end of the fuselage, the wings, the tail). More details can be found in [27].

Two remarks to conclude. Firstly, it should be noticed that α_x is a physical parameter, homogeneous to a conductivity (same units). This strongly suggests that its value should not be chosen as a pure arbitrary numerical parameter, but rather in function of physical parameters, as done in the two problems addressed in the above. Secondly, the CFS-PML is in general implemented in FDTD as a convolutional PML (CPML) [36], although an auxiliary equation implementation is possible as well. There is sometimes some confusion in the literature about the origin of its interesting possibilities. The CFS-PML can reduce the reflection of evanescent waves because of its stretching factor (3-15), not because of its convolutional

implementation, i.e. another implementation would produce the same beneficial effect on the evanescent waves.

III-6. Summary of the Perfectly Matched Layer

The PML has been viewed as a great advance in the field of the simulation of free space. In comparison with the numerous existing analytical ABCs, it permits a large reduction of the reflection of the outgoing waves in open problems solved by means of finite methods. Absorption of traveling waves is probably not better than that of such analytical ABCs as the Mur ABC or the Higdon ABC which was satisfactory (see next section on the actual performance of analytical ABCs). The principal advantage of the PML is its possibility of absorbing the evanescent fields which are present in almost all the problems of electromagnetism. In fact, for the reasons recalled in the above, the PML ABC may strongly reflect the evanescent fields in the discrete space, because its theoretical absorption of such waves is too high. This can be overcome by two means. The first one is to use a relatively thick PML where complementary reflections (Ramahi effect) from the successive rows of the discrete PML result in an overall reflection of evanescent fields which can be as small as desired, provided that the PML is thick enough. The other mean is the use of the CFS-PML which relies on a modified stretching factor. In many physical problems it permits the theoretical absorption of the evanescent fields to be the same as that of traveling waves, reducing then their reflection from the discrete PML. However, these remedies have some drawbacks. Choosing the best and optimum parameters of the PML is not evident and remains dependant on empirical knowledge, and on a certain a priori knowledge of the Physics of the problem to be solved. From this, the question of the absorption of evanescent fields remains a challenging question which prevents from considering the PML as an ideal ABC. For these reasons, it is clear that further researches in the field of absorbing boundary conditions remain of potential interest, mainly concerning the question of the evanescent waves.

IV. ABSORBING BOUNDARY CONDITIONS IN THE LAST DECADE

Despite the fact that the PML was considered as an effective ABC for solving any problems of electromagnetism, some innovative works have been published in the literature over the past 10-15 years, reporting novel ideas in the field of ABCs. For example, the lacunae-based ABC, introduced in the context of acoustic waves, has been the subject of several papers in years 2003-2012, from [51] to [52]. This ABC mainly relies on the fact that the acoustic or electromagnetic response to a compact in time source is lasting over a finite duration. By partitioning any time domain source into a set of short elementary sources, this permits the solution of open problems to be computed for any arbitrary long time using a finite domain, without reflection from the outer boundary. The principle of this ABC is attractive. However, there is no comparison with previous ABCs in the literature papers, nor example of application to problems of interest in electromagnetism. And it seems that the overall computational requirements of this ABC are far larger than those of the PML ABC.

In the following, we just review three ABCs published in the years 2000's for the absorption of electromagnetic waves. More precisely, two ABCs that were published almost simultaneously, the multiple absorbing surface [53] and the re-radiating boundary condition [54, 55]. They rely on the same fundamental principle. And a third ABC, the Huygens ABC [56], which is the generalization of the previous two. The HABC is promising in several aspects and could challenge the PML ABC, at least in some applications.

IV-1. The re-radiating boundary condition (rRBC)

The rRBC [54, 55] was introduced for use with the FDTD method. Its principle consists of generating a wave opposite to the outgoing wave leaving the computational domain, by means of a Huygens surface. If the generated wave were exactly opposite to the outgoing wave, the cancellation would be perfect, as represented in Fig. 4-1. Whatever may be the outer boundary placed behind the Huygens surface, there would be no backward reflection in the computational domain. In the papers [54, 55], the generation of the outgoing wave relies on the concept of teleportation of fields. The field one time step in the past and one space step backwards is "teleported" upon the Huygens surface where it is used to radiate the opposite field. This outgoing field is not exact, it is only an estimate, so that the cancellation is not perfect. From this the outgoing field is partially reflected. To improve the absorption, the computational domain in [54, 55] is ended with an impedance condition equivalent to a first order operator ABC.

There is neither derivation nor theoretical prediction in [54] and [55], only FDTD experiments are provided. The authors observed that the field outside the rRBC resembles the derivative on time of the outgoing field. They used the terms derivation and re-integration to characterize the direct and reverse effects of the rRBC. As it was derived later [56], the effect of the rRBC is indeed a derivation of the outgoing waves, and an integration of the ingoing waves.

Several experiments reported in [54, 55] show that the rRBC performance can be similar to that of the PML ABC. However, generalization of the conclusions of these experiments is questionable, because they were performed in a 2D domain with the electric field perpendicular to the domain. It is known that any ABC performs very well with this kind of problems, because no evanescent waves have to be absorbed. Especially, Higdon and Engquist-Majda ABCs also yield quite good absorption in that case [20]. In realistic FDTD applications where evanescent waves are present, results with the rRBC would be far poorer, because the teleportation used in this paper produces a total reflection of evanescent waves, as discussed in the following.

IV-2. The multiple absorbing surfaces (MAS)

The absorbing surface concept in [53] is introduced in the FDTD method by splitting the computational domain into a scattered-field region and a total-field region. There is no explicit reference to equivalent currents radiating a field opposite to the outgoing field. Nevertheless, what is done in this paper is equivalent to the generation of a wave opposite to

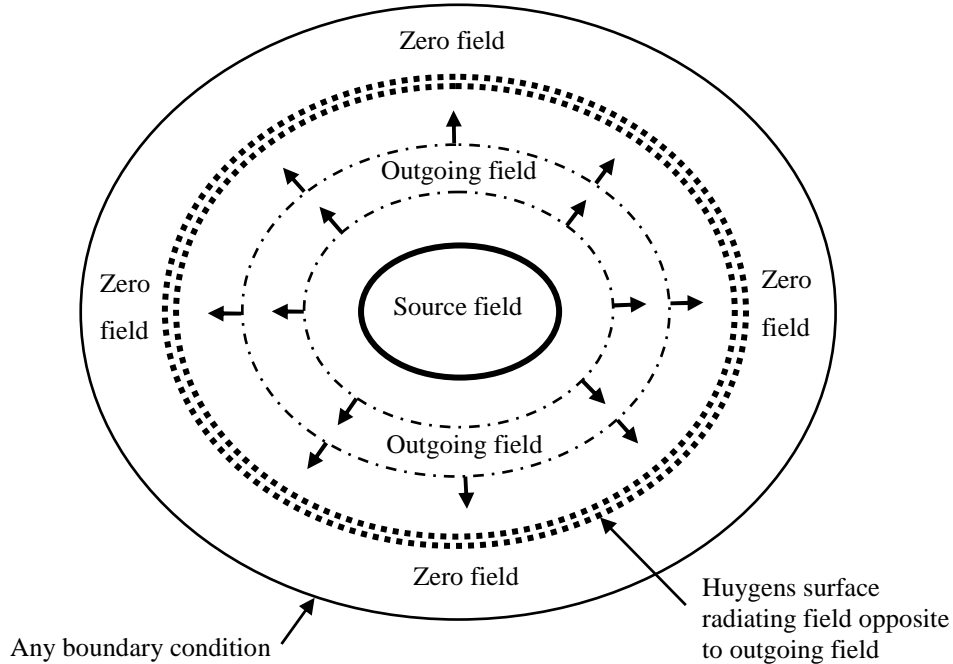


Fig. 4-1. The principle of the Huygens absorbing boundary condition.

the outgoing field by means of a Huygens surface, as in Fig. 4-1. The principal difference with the rRBC is that the outgoing field at the Huygens surface location is computed using the first order Higdon operator. This is a better estimate than the teleportation operator. The outer domain is closed with a PEC condition.

There are some theoretical derivations in the paper [53]. Especially, it is shown that the reflection produced by the ABC relying on the Higdon operator for estimating the outgoing field on the Huygens surface is identical to the reflection produced by the same Higdon operator used as a traditional ABC. The method then appears as just another implementation of the Higdon operators. The claimed advantage of the method is the easiness of stacking several surfaces to realize the equivalent of a high order Higdon operator. Several experiments show that the multiple absorbing surface permits an excellent absorption. However, the experiments are with a point source in a 2D domain where there is no evanescent waves, and with a scattering sphere with which results are provided only about the resonance frequency where the surrounding field is weakly evanescent. As with the rRBC, the experiments do not correspond to most situations of computational electromagnetics, because of lack of evanescent waves. Even by stacking a large number of absorbing surfaces, as long as only Higdon operators are used to estimate the outgoing field, the performance of the MAS method would be poor if the MAS surfaces were placed in the evanescent region.

IV-3. The basis and theory of the Huygens absorbing boundary condition (HABC)

The above two ABCs were developed independently and formulated in slightly different manners, but both rely on the

same basic principle that consists of cancelling the outgoing field leaving the domain by means of equivalent currents that radiate a field equal in magnitude and opposite in sign to the field to be cancelled (Fig. 4-1). This is a simple and attractive principle. These ABCs yield correct results in the test cases reported in the papers, but they do not significantly outperform such existing ABCs as the Mur or Higdon ABCs, because they do not absorb the evanescent fields. This prevents them to challenge the PML ABC in realistic calculations where there are always evanescent fields.

The MAS and rRBC have been generalized in paper [56], in the form of an ABC called the Huygens ABC (HABC). Theoretical properties of the Huygens ABC are derived in [56], both in continuous spaces and in the discrete FDTD space. The theory permits the observations and results in the rRBC and MAS papers to be explained and interpreted, and opens the way to the development of new families of ABCs that may challenge the PML. In this section, the principle of the HABC and the essential theoretical facts derived in [56] are summarized.

As the above MAS and rRBC, the HABC consists in generating an opposite wave to cancel the outgoing waves, by means of a Huygens surface (Fig. 4-1). In electromagnetics, a Huygens surface [16] permits sources to be replaced with currents sheets

$$\overline{J}_s = \overline{n} \times \overline{H}_i \quad (4-1a)$$

$$\overline{K}_s = -\overline{n} \times \overline{E}_i \quad (4-1b)$$

where \overline{n} is the unit vector normal to the surface, oriented in the direction opposite to the sources, and \overline{E}_i and \overline{H}_i are the fields that would exist upon the surface if the sources were present.

To realize a perfect HABC, E_i and H_i should be the opposites of the outgoing fields at the Huygens surface location, that is at the FDTD nodes where the HABC is implemented. In practice, things are different, because E_i and H_i cannot be known exactly. This can be viewed easily with the FDTD method. More fundamentally, in the continuous space this is because the field is discontinuous through the Huygens surface. For this reason, an estimate of the outgoing field is used in place of its exact, but unknown, value. Denoted as $\tilde{E}(x_c, t)$, the estimate at the Huygens surface location x_c is defined as a linear combination of the actual field values $E_a(x_c - \delta x_k, t - \delta t_k)$ present at several times and several locations close to the Huygens surface, on its inner side. For the $+x$ side of the Huygens surface, assumed as a parallelepiped box, this can be written as

$$\tilde{E}(x_c, t) = \sum_{k=1}^N a_k E_a(x_c - \delta x_k, t - \delta t_k) \quad (4-2)$$

where $\delta x_k \geq 0$, $\delta t_k \geq 0$, and

$$\sum_{k=1}^N a_k = 1 \quad (4-3)$$

With the FDTD method, where the field is known at mesh nodes separated with Δx and at times separated with Δt , this can be rewritten in terms of operators as

$$\tilde{E}(x_c, t) = P E_a(x_c, t) \quad (4-4)$$

with

$$P = \sum_{k=1}^N a_k K^{m_k} Z^{-n_k} \quad (4-5)$$

where K and Z^{-1} are the Higdon shift operators in space and time (see section 2-2), m_k and n_k are integers ($m_k \geq 0$, $n_k \geq 0$, with $m_k = n_k = 0$ excluded). Similar estimates as (4-2)-(4-5) are used for the H field, especially with the FDTD method where E and H are separated with $\Delta x/2$ in the direction normal to the Huygens surface [16].

The field behind the Huygens surface is the addition of the outgoing field with the field radiated by the Huygens surface. It is derived in [56] for an outgoing plane wave at incidence θ . It reads:

$$E_{\text{behind}} = \frac{\partial E_{\text{incident}}}{\partial t} \sum_{k=1}^N a_k \left(n_k \Delta t - \frac{\cos \theta m_k \Delta x}{c} \right) \quad (4-6)$$

This field is reflected by the PEC ending the domain (Fig. 4-1) and passes backwards through the Huygens surface. Derivation in [56] shows that the field reflected in the inner domain reads:

$$E_{\text{reflected}} = - \frac{1}{\sum_{k=1}^N a_k (n_k \Delta t + \cos \theta m_k \Delta x / c)} \int E_{\text{behind}} dt' \quad (4-7)$$

From (4-6) and (4-7), the Huygens surface acts as a derivator on time of the outgoing field, and as an integrator of the ingoing field propagating backwards. The waveform of the field reflected back into the inner domain is then the same as that of the outgoing wave, but its magnitude is multiplied with the product of the coefficients in (4-6) and (4-7). In other

words, the HABC formed with the Huygens surface and the PEC ending the domain is an ABC of reflection coefficient:

$$r = \frac{\sum_{k=1}^N a_k (\cos \theta m_k \Delta x - c n_k \Delta t)}{\sum_{k=1}^N a_k (\cos \theta m_k \Delta x + c n_k \Delta t)} \quad (4-8)$$

It can be easily shown [56] that this coefficient is nothing but the reflection coefficient of the operator (4-5) used as a traditional operator ABC on the outer boundary. This was also derived in [53] in the special case of the Higdon operator. The HABC is then just another implementation of the analytical operator ABCs in the form (4-5).

The teleportation operator of the rRBC is the special case of (4-5) $P_{tel} = K Z^{-1}$. For the MAS, the estimate is computed with the first order Higdon operator, which reads, from (2-29)

$$P_{H1} = K Z^{-1} + w K - w Z^{-1} \quad (4-9)$$

with w from (2-20). The reflection produced by the teleportation operator (called the elementary operator in [56]) is the special case ($N=1$, $a_1=1$, $m_1=n_1=1$) of (4-8):

$$r = \frac{(\cos \theta \Delta x - c \Delta t)}{(\cos \theta \Delta x + c \Delta t)} \quad (4-10)$$

whose zero reflection is at oblique incidence $\cos \theta = c \Delta t / \Delta x$. In the rRBC [54], the outer PEC is replaced with an impedance condition equivalent to a first order condition, with reflection (2-9). The overall reflection is then the product of the two reflection coefficients. This permits (see [56]) the interpretation of some results reported in [54, 55]. For the MAS surface, using (4-9) into (4-8) yields, as expected, the reflection from a Higdon operator used as a traditional ABC, that is (2-9).

Obviously, the second order Higdon operator, which is also a special case of (4-5), can be used with the HABC. It would produce a reflection equal to the square of (2-9). The corresponding P_{H2} operator is given in [56].

The results in Fig. 4-2 from [56] demonstrate the derivation (4-6) and re-integration (4-7) of the outgoing pulse by the HABC surface. The experiment was in 1D (equivalent to 3D at normal incidence) with the elementary operator used in the rRBC whose reflection is (4-10) for $\theta = 0$. It is clear that the pulse behind the HABC is the derivative of the Gaussian incident pulse, which is then re-integrated as it passes back through the HABC, with a final magnitude in accordance with (4-10).

A remark should be done here about special cases of operator (4-5) where the first derivative is replaced with the second derivative in (4-6), and the integral in (4-7) replaced with a double integral on time. The reflection then differs from (4-8), but it remains equal to the reflection from the same operator used as a traditional ABC. More details are available in [56].

The reflection coefficient (4-8) is that of pure traveling waves. The reflection of evanescent waves with wavenumbers (2-10)-(2-11) has been derived in [56] as well. It reads

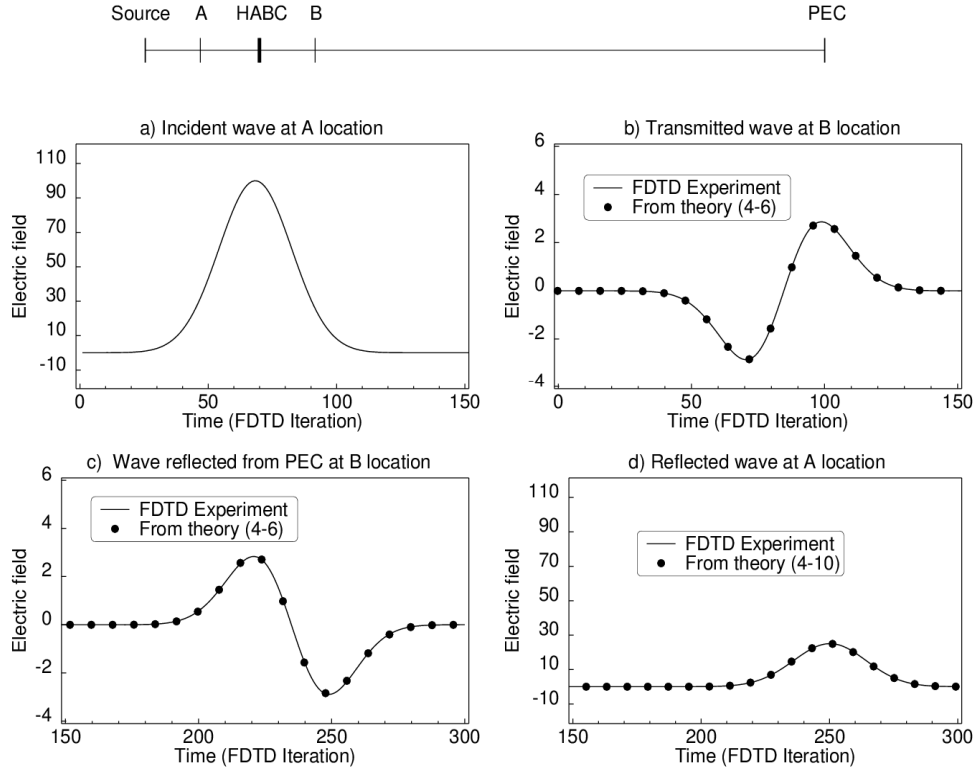


Fig. 4-2. Reflection from the Huygens ABC. A comparison of theory with a FDTD experiment. The wave is observed at A and B on the two sides of the HABC. The distances from the source to A, HABC, B, and PEC are 5, 10, 15, and 60 FDTD cells of 5 cm, respectively.

$$r = \frac{\sum_{k=1}^N a_k [j(\cosh \chi \cos \theta m_k \Delta x - c n_k \Delta t) - \sinh \chi \sin \theta m_k \Delta x]}{\sum_{k=1}^N a_k [j(\cosh \chi \cos \theta m_k \Delta x + c n_k \Delta t) - \sinh \chi \sin \theta m_k \Delta x]} \quad (4-11)$$

which is again, as it can be shown, the reflection from the same operator used as a traditional ABC. Obviously, (4-8) is nothing but the special case $\chi=0$ of (4-11). In the case of strongly evanescent waves, where $\cosh \chi \gg 1$, (4-11) yields $r = 1$, so that the reflection is total from the HABC with any operator (4-5), especially with Higdon operators. This means that the HABC relying on (4-5) suffers from the same drawback as the Higdon operator ABC, it cannot absorb the evanescent waves that are present in most problems of electromagnetics.

Fig. 4-3 from [56] illustrates the equivalence of the HABC with its operator implemented as a traditional analytical ABC. It reports experiments with a parallel plate waveguide, using Higdon operators of orders 1 and 2, implemented either as an operator ABC or as a Huygens ABC. It can be seen that the results of the two implementations are superimposed, both in the traveling region above the cutoff frequency 3.75 GHz and in the evanescent region where the reflection is total (the low frequency plateau is 6 dB below total reflection because of the natural decrease of the evanescent waves over the separation between the source and the ABCs).

IV-4. Implementation of the HABC in Cartesian coordinates and extensions of the HABC

The Fig. 4-1 summarizes the theoretical principle of the HABC. However, it must be slightly modified in practice because the Huygens surface only radiates an estimate of the outgoing field. Especially in Cartesian domains where the HABC surface is a rectangle in 2D, or a parallelepiped in 3D. At the corners or edges the direction of the normal to the surface is discontinuous (discontinuity of orientation by $\pi/2$). From this, the outgoing field estimated by means of an operator is discontinuous. This results in the generation of a spurious source of field in the vicinity of corners and edges. A solution has been found [57] by adding what is called extensions to the physical Huygens surface. They are represented in Fig. 4-4 in the 2D case. The four sides of the HABC are extended up to the outer PEC ending the domain. Similarly, in 3D the six faces of the HABC are extended up to the PEC. The Huygens currents (4-1) are applied on the extensions in the same way as on the normal sides of the HABC. With this disposal, it can be seen [57] that there is no discontinuity of the radiated field in the different regions defined by the HABC and the extensions.

More details can be found in [57] where numerical experiments illustrate the need of the extensions. The practical implementation of the extensions is a little change in the encoding since it just consists of extending some loops. The need of extensions was not found when the work [56] was

done, because the experiments were only in 2D without corners (HABC at the end of a waveguide). In the rRBC and MAS papers the need of extensions is not mentioned as well. However, although the rationale for the authors to do this is not reported, it seems that in [54, 55] the Huygens planes were extended up to the outer boundary ending the domain in the numerical experiments.

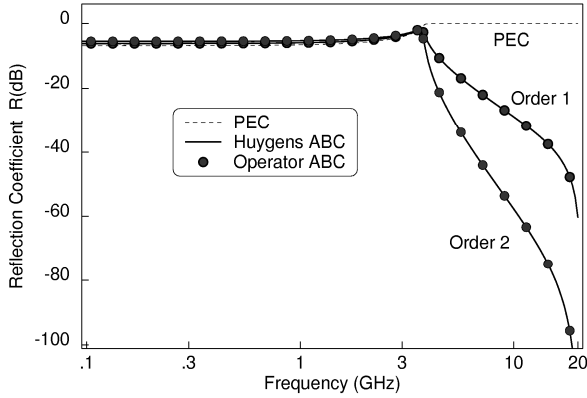


Fig. 4-3. Comparison of the reflection coefficients computed using either an operator ABC or a Huygens ABC at the end of a parallel-plate waveguide. In both cases the operators are either the 1-order Higdon operator or the 2-order Higdon operator. The PEC result is with the waveguide ended with a PEC alone, without ABC.

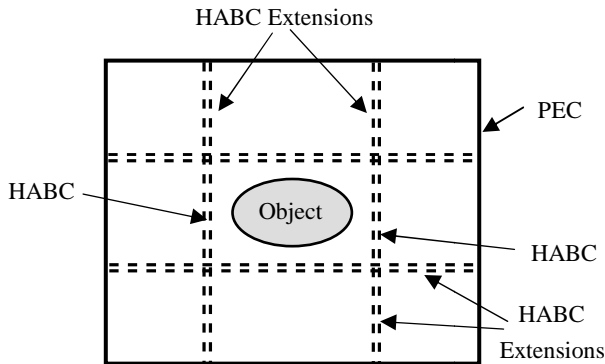


Fig. 4-4. The extensions of the HABC. The six faces of the Huygens surface box (in 3D) are extended up to the outer PEC of the computational domain.

IV-5. The potential interest of the HABC

As shown in the above the HABC is nothing but another implementation of analytical ABCs, as the Mur or Higdon ABCs or any operator in the form (4-5). From this, one may think that it is of little interest. Indeed, this is not true, the HABC has some characteristics that render it of potential high interest for numerical electromagnetics. Mainly the following two:

1/ As proposed in the pioneering work of the MAS [53], it is possible to stack several HABCs. The reflection is then the product of the individual reflections. Stacking for instance three first order Higdon HABCs is equivalent to a single third order Higdon operator. There is no gain, in theory, but the implementation is simpler, and the stability may be better, as it is claimed in [53]. However, the true interest in stacking several HABCs is not in staking numerous HABCs only designed for the absorption of pure traveling waves, as done in

[53]. The true interest is indeed in the possibility of easily stacking operators designed for the traveling waves with operators designed for the evanescent waves. This is demonstrated in the following.

2/ The HABC can be placed in front of another boundary condition, by just replacing the PEC in Fig. 4-1, with the other ABC. This permits easy combinations with such ABCs as the PML or a simple and rather exotic, but effective, real stretch of coordinates (see in the following). Combinations of several ABCs are of high potential interest because they render possible combinations of one ABC designed for the traveling waves with another designed for the evanescent waves, as demonstrated in the following.

IV-6. A HABC for both traveling and evanescent waves

In the framework of analytical ABCs, it seems only the Betz-Mittra operator (2-49) has been reported for the absorption of evanescent fields. In [56], another simple operator has been used to absorb the evanescent field at the end of a waveguide. It consists in writing that the field at the boundary, or at the Huygens surface node with the HABC implementation, is the field one cell in the interior multiplied with a coefficient $\beta < 1$. This is an operator designed for waves evanescent in the direction perpendicular to the boundary, with the direction of the propagation of the phase parallel to the boundary. In terms of operator, this reads:

$$P_{eval} = \beta K \quad (4-12)$$

With the phase propagation parallel to the boundary ($\theta = \pm\pi/2$), the reflection coefficient of (4-12) is derived in [56]. It reads

$$r = -\frac{1 - \beta e^{\frac{\omega}{c} \sinh \chi \Delta x}}{1 - \beta e^{-\frac{\omega}{c} \sinh \chi \Delta x}} \approx -\frac{1 - \beta(1 + \omega \sinh \chi \Delta x / c)}{1 - \beta(1 - \omega \sinh \chi \Delta x / c)} \quad (4-13)$$

which is not a special case of (4-11) because (4-3) used to derive (4-11) does not hold with (4-12). Reflection (4-13) vanishes if

$$\beta = e^{-\frac{\omega}{c} \sinh \chi \Delta x} \quad (4-14)$$

With a parallel plate waveguide of cutoff frequency ω_c , the product $\omega \sinh \chi$ is given by (3-21) when $\omega \ll \omega_c$. Considering the TM_1 mode and using this $\omega \sinh \chi$ into (4-14) yields the value of β which cancels the reflection of the evanescent waves at low frequency:

$$\beta = e^{-\frac{\pi}{a} \Delta x} \quad (4-15)$$

Results provided in [56] show that the operator (4-12) with β from (4-15), implemented either as a traditional ABC or as a HABC, does absorb very well the evanescent waves of the TM_1 mode. The operator (4-12) can be squared to obtain a second-order operator (see [56]). By stacking several HABCs, some relying on the Higdon operator and some on (4-12), both the traveling waves and the evanescent waves are absorbed. This is illustrated in Fig. 4-5 from [56] where either two or four HABCs are used. The best result in the figure was computed with two second order HABCs for traveling waves, and two second order HABCs for evanescent waves, which is equivalent to an eight-order analytical ABC, with four orders

devoted to the traveling waves, and four to the evanescent waves. The reflection is then roughly similar to that obtained with an eight-cell optimized CFS-PML.

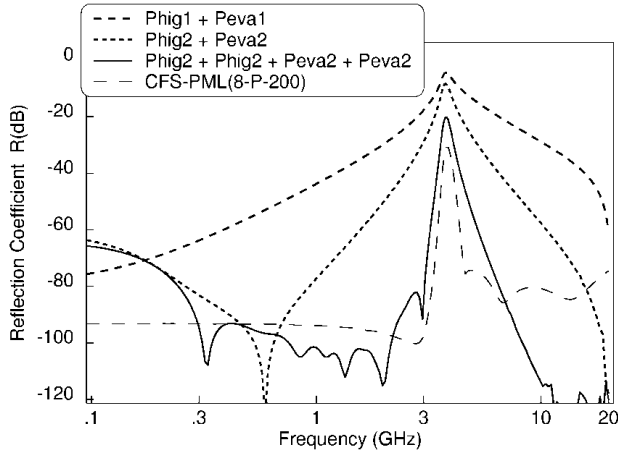


Fig. 4-5. Reflection from the end of a waveguide using various combinations of Higdon operators (first order Phig1 and second order Phig2) with evanescent operators (4-12) (first order Peva1 and second order Peva2).

IV-7. Combination of the HABC with the PML

It is easy to place a HABC in front of a PML ABC. An experiment is reported in [56] with the same waveguide as above. Here the HABC is used to absorb the TM_0 mode of the parallel plates which is a traveling mode at any frequency (no cutoff). The CFS-PML optimized for the TM_1 mode cannot absorb the traveling waves below the cutoff (it is there just a real stretch of coordinate). In principle, this situation could be addressed by adding some cells of PML with a normal stretching factor to absorb the TM_0 mode. However, a more elegant solution consists in adding a HABC with the Higdon operator in front of the PML. This is simpler and probably less demanding in computational resource. The reader is referred to [56] to see more details on this experiment.

IV-8. The stretched-mesh HABC (SM-HABC)

The SM-HABC [58] is another illustration of the possibility of combining the HABC with another ABC. It consists in using a HABC for the absorption of traveling waves and a stretched mesh (SM) for the absorption of evanescent waves. The SM ABC is not a new ABC, it is just a strongly stretched FDTD mesh used to fill a large enough domain outside the HABC, in such a way that the evanescent waves can decrease to a negligible level. Stretched meshes were used in the past to reduce the overall number of FDTD cells while preserving a large physical domain. However, the stretching was severely limited when using ABCs on the outer boundary, because of the reflection of high frequencies from the large cells. Conversely, by placing the HABC in front of the stretched mesh, the high frequency traveling waves are absorbed by the HABC before entering the stretched mesh (more precisely, the high frequencies are reflected by the stretched mesh, which plays the role of the outer PEC in Fig. 4-1). Only evanescent waves are present behind the HABC, in the stretched domain. Since in most cases the evanescent waves are low frequency waves, a strong stretch can be applied without penalty, so that

the stretched mesh can be reduced to a few FDTD cells while preserving a large enough physical domain. The principle of the SM-HABC is represented in the Fig.4-6. A scattering object is surrounded with the HABC and its extensions. A coarse mesh fills the space outside the closed part of the HABC.

The SM-HABC is well suited to such problems as the interaction of an incident wave with a scattering structure, where the high frequencies are traveling waves and the low frequencies are evanescent waves, with a transition about the fundamental resonance of the structure. The high frequencies are then absorbed by the HABC which relies on the first order Higdon operator in [58], and the low frequencies decrease in a natural manner in the large domain outside the HABC. Experiments with this kind of problems are reported in [58]. However, the concept could be more widely applied in numerical electromagnetics since in most problems the evanescent waves are low frequency waves, allowing then their attenuation by means of a stretched mesh.

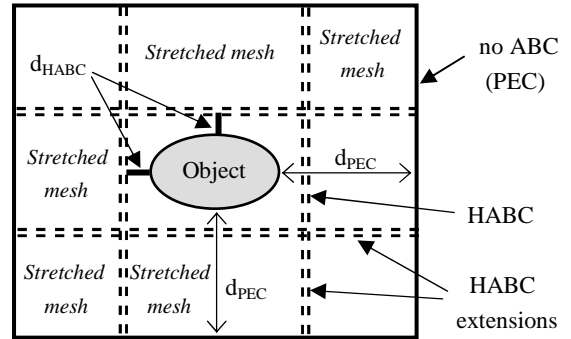


Fig. 4-6. The principle of the SM-HABC. The HABC (closed surface) is surrounded with a stretched mesh (geometrical expansion of the FDTD cell). The HABC is placed d_{HABC} from the object and the outer PEC d_{PEC} from the object.

The experiments reported in [58] shows that the Higdon-based HABC can very well absorb the traveling waves, even when it is placed in the close vicinity of a scattering structure. This is illustrated by the Fig. 4-7 where the HABC is placed several distances from a 100-10-0-cell PEC plate stricken by an incident pulse (a Gaussian pulse or a Unit-step pulse). A large domain filled with a uniform mesh surrounds the HABC in order that the evanescent waves decrease to a negligible value ($d_{PEC} = 200$ cells is the distance between the 100-10-0-cell plate and the outer PEC). Even with the HABC placed only three FDTD cells away the object ($d_{HABC} = 3$ cells in the figure), there is no visible reflection of the traveling waves (taking account of the delay of propagation over 400 cells of 1 cm, if a reflection were present it would appear about time 20 ns in the figure). These results show that the first order Higdon ABC can achieve a very good attenuation of traveling waves, better than was previously believed. The HABC implementation permits the absorptions of traveling and evanescent waves to be decoupled. This clearly shows the high performance of the operator, conversely to the case where it is implemented as a traditional ABC, on the outer

boundary, where the reflections of traveling and evanescent waves cannot be clearly distinguished.

In [58], the cell size in the stretched mesh grows geometrically from the HABC to the outer PEC, i.e. the cell is multiplied with a factor g from one cell to the next. The stretch can be large, resulting in a dramatic reduction of the number of cells needed to fill the domain outside the HABC. This is illustrated by the Fig. 4-8 where the same problem as in Fig. 4-7 is addressed, i.e. the field on the surface of a 100-10-0-cell plate. The HABC is three cells from the plate, and ng stretched cells outside the HABC replace the uniform mesh of Fig. 4-7 (the physical domain is identical, equivalent to 200 uniform cells). As can be seen, the results remain acceptable, even with a small number of stretched cells in place of the large number of uniform cells. In other words, 3 strongly stretched cells can replace 196 uniform cells (the stretch begins one cell away from the HABC which is 3 cells from the object). The computational requirements, memory and CPU times, are then dramatically reduced in comparison with the uniform mesh.

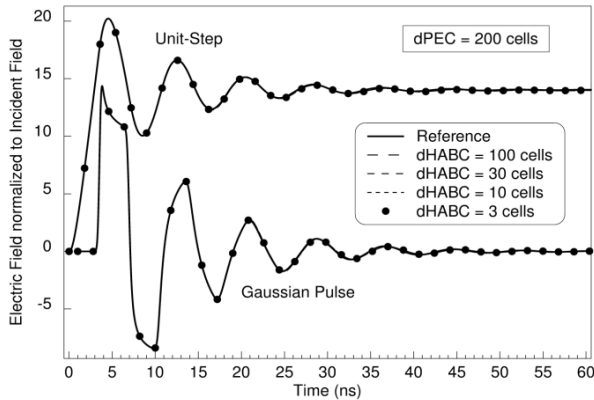


Fig. 4-7. Electric field on the surface of a 100-10-0-cell plate, computed with the HABC placed 3, 10, 30, 100 cells from the plate, a uniform mesh in the whole domain, and the outer PEC 200 cells from the plate.

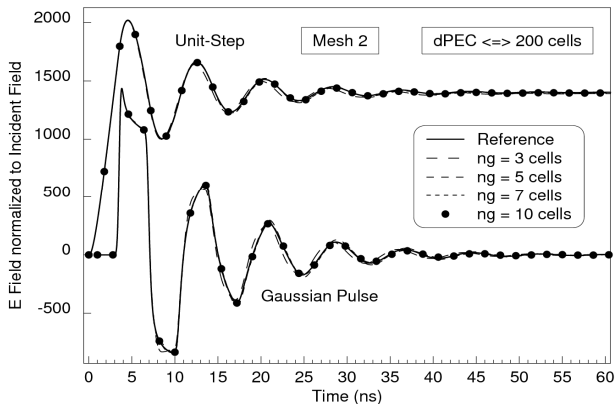


Fig. 4-8. Electric field on a 100-10-0-cell plate computed with the HABC 3 cells from the plate ($d_{HABC} = 3$ cells) and four stretched meshes ($ng = 3, 5, 7, 10$ cells) behind the HABC (mesh 2 defined in [58]). In all the cases the plate-PEC separation equals 2 m which is equivalent to 200 uniform cells.

The achievement in Fig. 4-8 is possible because the high frequency traveling waves are absorbed by the Higdon-based

HABC in front of the stretched mesh. With the traditional implementation as an analytical ABC on the outer boundary, using a widely stretched mesh is not possible, since then the high frequency waves cannot propagate through the large FDTD cells, and then cannot reach the Higdon operator. This is clear in the Fig. 4-9, where the same problem as in Fig. 4-8 is addressed, except that the HABC is replaced with the Higdon ABC implemented on the outer boundary, in place of the outer PEC. Then the high frequencies are reflected backwards by the stretched mesh, resulting in the strong spurious reflection visible in Fig. 4-9. Thus, comparing Fig. 4-8 with Fig. 4-9 clearly demonstrates the high interest of the HABC implementation of operator ABCs in comparison with the traditional implementation. The possibility of placing the HABC in front of another ABC is a unique feature that opens the way to new achievements in the matter of ABCs.

An example of application of the SM-HABC to the airplane problem previously addressed with the Higdon operator in Fig. 2-7 and with the CFS-PML in Fig. 3-10 is reproduced in Fig. 4-10. It can be seen that the computed results are correct with a small number of stretched cells ($ng = 3-5$). The overall computational domain size and CPU time are very similar to the ones of the CFS-PML calculations in Fig. 3-10. The SM-HABC cannot really outperform the CFS-PML, but it can challenge it, with the advantage of a simpler implementation.

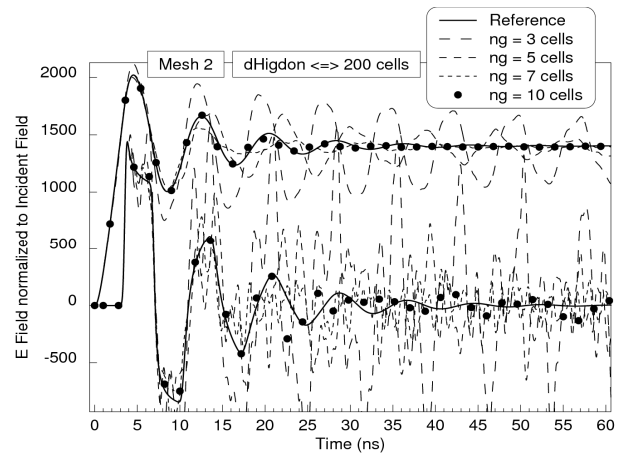


Fig. 4-9. Electric field on a 100-10-0-cell plate computed with four stretched meshes (the same as in Fig. 4-8) and a Higdon operator ABC placed on the outer boundary. In all the cases the plate-ABC separation equals 2 m which is equivalent to 200 uniform cells.

IV-9. Summary and discussion on the HABC

Although it is in principle just another implementation of analytical ABCs, the HABC is much more for two reasons. Firstly, it allows easy combinations of operators devoted to traveling waves with operators devoted to evanescent waves. Secondly, it can be placed in front of another ABC and then combined with a PML, or with more innovative ABCs such as the simple, but effective, real stretch of coordinates.

From this, novel ABCs that can really challenge the PML ABC can be elaborated. As the SM-HABC introduced in [58] for wave-structure interaction problems, but that could be applied as well to other problems where evanescent waves are present at low frequency (as waveguide problems for instance). Moreover, it seems that the SM-HABC has rather

more potential than the CFS-PML. Because the optimization of the CFS-PML is more problem dependant. It assumes that the frequency spectrum is like in Fig. 3-9, with the optimum parameter α_x depending on the relationship (3-21) for waveguide problems, or (3-24) for interaction problems. In both cases, the relationship depends on a parameter, the mode in (3-21) or the parameter p in (3-24). Conversely the SM-HABC only relies on the fact that evanescent fields are low frequency fields, so that it can be suited to all the modes in a waveguide problem and can even absorb low frequency traveling waves (as the TM_0 mode). Although the CFS-PML could in principle address any situation by varying its α_x parameter within it, the SM-HABC appears as superior. More numerical experiments should be performed to conclude and compare more extensively the two ABCs in situations close to realistic applications, but the less restrictive assumptions of the SM-HABC are, a priori, a favorable feature.

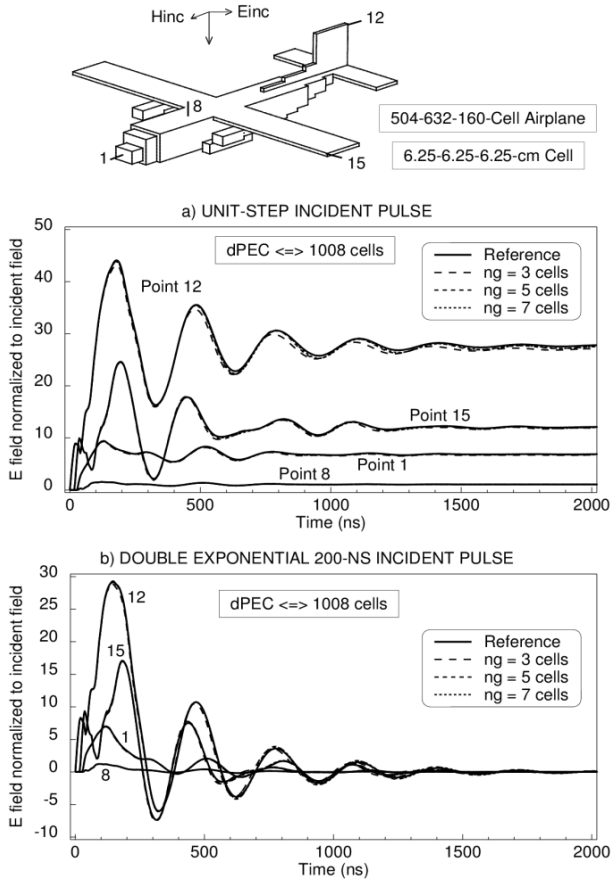


Fig. 4-10. Electric field on the surface of a 504-632-160-cell airplane with SM-HABCs of 3, 5, 7 stretched cells, for a unit-step and a double-exponential pulse.

On the other side, the HABC is only described in [56-58] for the simulation of free space in a vacuum. Obviously it could also be used with little change in isotropic and non dispersive media. However, its extension to more complex media is far from trivial. Finding analytical ABCs for general media has been a challenging and mainly unsolved question in the past. Thus, at present there is no available operator to estimate the outgoing field in complex media. This is a serious

limitation of the HABC in contrast with the PML which has been relatively easily extended to any kind of media, from lossy media to metamaterials.

V. CONCLUSIONS AND PROSPECTS

Absorbing boundary conditions are needed to solve most problems of numerical electromagnetics with such finite methods as the FDTD or the FEM. They have been the subject of researches almost continuously over the past 40-45 years. Several analytical ABCs were developed in the years 1970-1990. However, despite numerous works, little progress was observed during this period. The PML ABC introduced in 1994 rapidly appeared as a breakthrough advance because it can outperform previous ABCs in the two principal aspects of the simulation of free space: 1/ the reduction of the reflection from the ABC, which means a better accuracy of the calculations, and 2/ the reduction of the overall computational cost of the calculations. In addition, the PML has been extended easily to any media, including dispersive, anisotropic, and metamaterial media. However, even if the PML is effective and universal, the more recently introduced Huygens ABC enriches the range of available ABCs. It permits re-use of the existing analytical ABCs in a different and successful manner, and subsequently permits the design of ABCs that can challenge the PML, and may outperform it in some problems, especially regarding the question of the simplicity.

What is clear nowadays is that the problem of the simulation of free space has not been well understood in the years 70 and 80. The researches were focused on the improvement of the absorption of traveling waves, as if only traveling wave existed. In reality, evanescent waves are present in most problems. This explains why there has not been significant progress during this period. The reason of the effectiveness of the PML and HABC mainly lies in their ability to absorb the evanescent fields. With the PML by means of complementary reflections (Ramahi effect), or by using an optimized CFS stretching factor. With the HABC by means of operators designed to this end, or by means of combinations with such non conventional ABCs as a simple real stretch of coordinates.

What may explain why the workers have not paid much attention to the evanescent waves in the past decades is the absence of the general evanescent solutions of the Maxwell equations in the textbooks on electromagnetism, for instance in Stratton or Van Bladel textbooks. This lack of the general waveform of the electromagnetic field has been an obstacle to interpret the reflection from PMLs, in the context of which the evanescent solutions of the Maxwell equations had to be derived from scratch [40] in the 2D case (appendix A). This probably has been an obstacle as well for the development of effective analytical ABCs in the 70s and 80s.

Finally, although nowadays the simulation of free space is considered as satisfactory in most situations, mainly using the PML ABC, progress is endless and there is still room for works in the field of ABCs. With such objectives as the simplicity of the implementation, the simplicity of the settings of the ABC, or the reduction of the sensitivity of the results to the parameters of the problem. In a vacuum, which is the most

current medium in applications, the Huygens ABC opens the way to new researches, mainly because of its unique feature that permits easy combinations of different ABCs. However, further researches can only succeed if one keeps in mind the central question in the matter of ABC research, which is, once again, the fact that the evanescent waves have to be absorbed. This in turn implies that a clear and explicit knowledge of the general solutions of the Maxwell equations is available.

APPENDIX A

EVANESCENT SOLUTIONS OF THE MAXWELL EQUATIONS

Let us consider the equation of dispersion of the Maxwell equations in the 2D case:

$$k_x^2 + k_y^2 = \frac{\omega^2}{c^2} \quad (\text{A-1})$$

Beside the usual solution ($k_x = \omega \cos\theta/c$, $k_y = \omega \sin\theta/c$), the following more general solution also satisfies the equation

$$k_x = \frac{\omega}{c} (\cosh \chi \cos \theta + j \sinh \chi \sin \theta) \quad (\text{A-2})$$

$$k_y = \frac{\omega}{c} (\cosh \chi \sin \theta - j \sinh \chi \cos \theta) \quad (\text{A-3})$$

where θ and χ are free parameters. The waveform $\exp(j\omega t - jk_x x - jk_y y)$ of the E (or H) field is then in the form

$$E = E_0 e^{j\omega \left[t - \frac{\cosh \chi}{c} (x \cos \theta + y \sin \theta) \right]} e^{-\frac{\omega}{c} \sinh \chi (y \cos \theta - x \sin \theta)} \quad (\text{A-4})$$

By the rotation of coordinates defined in the figure, this can be rewritten as

$$E = E_0 e^{j\omega \left[t - \frac{\cosh \chi}{c} X \right]} e^{-\frac{\omega}{c} \sinh \chi Y} \quad (\text{A-5})$$

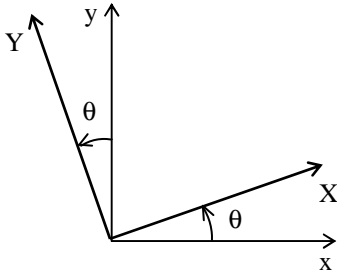


Fig. A-1. Rotation of coordinates θ .

Equation (A-5) is the waveform of a plane wave whose phase propagates with speed $\cosh\chi/c$ in direction X forming the angle θ with direction x , and whose magnitude decreases in direction Y perpendicular to X . Quantity $\chi \in [-\infty, +\infty]$ is the evanescence parameter. The case $\chi = 0$ is the special case of the pure traveling waves.

Some results are derived in [40] about the reflection of the evanescent waves from an interface, which also hold for the reflection by an ABC. For an incident wave whose phase propagates in direction θ the phase of the reflected wave propagates in direction $\pi - \theta$, as that of a pure traveling wave. And the evanescence parameter χ of the reflected wave is equal in magnitude, but opposite in sign, to that of the incident wave.

The 2D solutions of the Maxwell equations are sufficient to compute the reflection coefficients from an analytical ABC or from a PML, because ABC problems are mainly 2D problems (at least as long as the medium is isotropic).

APPENDIX B

EVANESCENT FIELDS IN THE VICINITY OF SCATTERING STRUCTURES

Apparently, in the literature or textbooks, there is nothing about the general form of the evanescent fields surrounding structures stricken by an incident wave. Only canonical cases are addressed. In order to interpret the observed reflection from PMLs, it was assumed in the work [40] that the low frequency field around PEC structures is composed of evanescent waves whose evanescence parameter χ is connected with the frequency by the relationship:

$$\omega \sinh \chi = p \frac{c}{w} \quad (\text{B-1})$$

where p is a parameter of the order of unity and w is the (largest) size of the structure. The relationship was deduced from the fact that the evanescent fields strongly decrease over a distance of the order of the largest size of scattering structures. Taking account of the coefficient of decrease of the evanescent waves (appendix A, formula A-5), this reasoning yields:

$$e^{-\frac{\omega}{c} \sinh \chi w} = e^{-p} \quad (\text{B-2})$$

or equivalently (B-1). The formula (B-1) is fundamental to optimize the CFS-PML (its α_x parameter). It could also be used to design operators for the absorption of evanescent waves in scattering calculations.

Formula (B-1) can be viewed as obtained empirically. However, more recently the question has been investigated theoretically and a rigorous formula derived in the special case of symmetric 2D structures [59]. In that case, the spectrum of the plane waves evanescent in the direction perpendicular to the largest size w presents peak values for the following χ parameters

$$\omega \cosh \chi_m = (2m + 1) \frac{\pi c}{w} \quad (\text{B-3})$$

with magnitudes of the peaks decreasing as m grows. Since the resonance frequency is $\omega_0 = \pi c/w$, far below the resonance $\cosh\chi \gg 1$ holds. From which $\cosh\chi \sim \sinh\chi$ and then (B-3) agrees well with (B-1). It can be noticed that (B-3) is the same as the formula that holds for a parallel plate, with just the object size w in place of the waveguide width.

REFERENCES

- [1] K. S. Yee, "Numerical solution of initial boundary value problems involving Maxwell's equations in isotropic media", *IEEE Trans. Ant. Propag.*, vol. 14, pp. 302-307, 1966.
- [2] D.E. Merewether, "Transient currents induced on a metallic body of revolution by an electromagnetic pulse", *IEEE Trans. Electrom. Compat.*, vol. 13, pp. 41-44, 1971.
- [3] R. Holland, "THREDE: A free-field EMP coupling and scattering code", *IEEE Trans. Nuc. Sc.*, vol. 24, pp. 2416-2421, 1977.

- [4] J.-P. Bérenger, "A perfectly matched layer for the absorption of electromagnetic waves", *J. Comput. Phys.*, vol. 114, pp. 185-200, 1994.
- [5] J.-P. Bérenger, "Etude préalable à la simulation par calcul de l'action de l'EMP sur un aéronef. Mise au point d'une cavité anéchoïde numérique", note technique DGA/ETCA/DET n° 390, Juillet 1977.
- [6] J.-P. Bérenger, "Calcul de la diffraction à l'aide d'une méthode aux différences finies " Actes du colloque CEM83, CNFRS-URSI, Trégastel, France, Juin 1983.
- [7] R. Holland, J.R. Williams "Total-field versus scattered-field finite-difference : a comparative assessment ", *IEEE Trans. Nuc. Sc.*, vol. 30, pp. 4583-4588, 1983.
- [8] B. Engquist, A. Majda, "Radiation boundary condition for the numerical simulation of waves", *Math. Comput.*, vol. 31, pp. 629-651, 1977.
- [9] R. Higdon, "Absorbing boundary conditions for difference approximations to the multi-dimensional wave equation", *Math. Comput.*, vol. 47, pp. 437-459, 1986.
- [10] R. Higdon, "Numerical absorbing boundary conditions for the wave equation", *Math. Comput.*, vol. 49, pp. 65-90, 1987.
- [11] A. Bayliss, E. Turkel, "Radiation boundary conditions for wave-like equations", *Com. Pure App. Math.*, vol. 33, pp. 707-725, 1980.
- [12] A. C. Reynolds, "Boundary conditions for the numerical solution of wave propagation problems", *Geophysics*, vol. 43, pp. 1099-1110, 1978.
- [13] R. G. Keys, "Absorbing boundary conditions for acoustic media", *Geophysics*, vol. 50, pp. 892-902, 1985.
- [14] Z.P. Liao, H.L. Wong, B.P. Yang, Y.F. Yuan, "A transmitting boundary for transient wave analyses", *Scientia Sinica (A)*, vol. 27, pp. 1063-1076, 1984.
- [15] G. Mur, "Absorbing boundary conditions for the finite-difference approximation of the time-domain electromagnetic-field equations", *IEEE Trans. Electrom. Compat.*, vol. 23, pp. 377-382, 1981.
- [16] A. Taflove, S. Hagness, *Computational Electrodynamics: The Finite-difference Time-domain Method*, Artech House, Boston, 2000.
- [17] S. Gedney, *Introduction to the Finite-Difference Time-Domain (FDTD) Method for Electromagnetics*, Morgan and Claypool, Los Angeles, 2011.
- [18] L. Halpern, L.N. Trefethen, "Wide-angle one-way wave equations", *J. Acoust. Soc. Amer.*, vol. 84, pp. 1397-1404, 1988.
- [19] P. A. Tirkas, C. A. Balanis, R. A. Renaut, "Higher order absorbing boundary conditions for the finite-difference time-domain method", *IEEE Trans. Ant. Propag.* vol. 40, pp. 1215-1222, 1992.
- [20] J. Blaschak, G. Kriegsmann, "A comparative study of absorbing boundary conditions", *J. Comput. Phys.*, vol. 77, pp. 109-139, 1988.
- [21] L. T. Simpson, R. Holland, S. Arman, "Treatment of late time instabilities in finite-difference EMP scattering codes", *IEEE Trans. Nuc. Sc.*, vol. 29, pp. 1943-1948, 1982.
- [22] A. Taflove, E. Brodwin, "Numerical solution of steady-state electromagnetic scattering problems using the time-dependent Maxwell's equations", *IEEE Trans. Micr. Th., Techn.*, vol. 23, pp. 623-630, 1975.
- [23] A. Taflove, E. Brodwin, "Computation of the electromagnetic fields and induced temperatures within a model of the microwave-irradiated human eye", *IEEE Trans. Micr. Th., Techn.*, vol. 23, pp. 888-896, 1975.
- [24] K.K. Mei, J. Fang, "Superabsorption. A method to improve absorbing boundary conditions", *IEEE Trans. Ant. Propag.*, vol. 40, pp. 1001-1010, 1992.
- [25] V. Betz, R. Mittra, "Compaision and evaluation of boundary conditions for absorption of waves in an FDTD simulation", *IEEE Micr. Guid. Waves Lett.*, vol. 2, pp. 499-501, 1992.
- [26] J.-P. Bérenger, *The Perfectly Matched Layer for Computational Electromagnetics*, Morgan and Claypool, Los Angeles, 2007.
- [27] J.-P. Bérenger, "An optimized CFS-PML for wave-structure interaction problems", *IEEE Trans. Electrom. Compat.*, vol. 54, pp. 352-358, 2012. doi: 10.1109/TEM.C.2011.2178852.
- [28] O.M. Ramahi, "Complementary operators: a method to annihilate artificial reflections arising from the truncation of the computational domain in the solution of partial differential equations", *IEEE Trans. Ant. Propag.*, vol. 43, pp. 697-704, 1995.
- [29] O.M. Ramahi, "Complementary boundary operator for wave propagation problems", *J. Comput. Phys.*, vol. 133, pp. 113-128, 1997.
- [30] O.M. Ramahi, "The concurrent complementary operators method for FDTD mesh truncation", *IEEE Trans. Ant. Propag.*, vol. 46, pp. 1475-1482, 1998.
- [31] J.-P. Bérenger, "A perfectly matched layer for the free-space simulation in finite-difference computer codes", *Annals of Telecom.*, vol. 51-1, pp. 39-46, 1996.
- [32] W.C. Chew, W.H. Weedon, "A 3D perfectly matched medium from modified Maxwell's equations with stretched coordinates", *Micr. Opt. Technol. Lett.*, vol. 7-13, pp. 599-604, 1994.
- [33] J.-P. Bérenger, "Three-dimensional perfectly matched layer for the absorption of electromagnetic waves", *J. Comput. Phys.*, vol. 127, pp. 363-379, 1996.
- [34] Z.S. Sacks, D. M. Kingsland, R. Lee, J.-F. Lee, "A perfectly matched anisotropic absorber for use as an absorbing boundary condition", *IEEE Trans. Ant. Propag.*, vol. 43, pp. 1460-1463, 1995.
- [35] S.D. Gedney, "An anisotropic perfectly matched layer-absorbing medium for the truncation of FDTD lattices", *IEEE Trans. Ant. Propag.*, vol. 44, pp. 1630-1639, 1996.
- [36] J.A. Roden, S. D. Gedney, "Convolutional PML (CPML): An efficient FDTD implementation of the CFS-PML for arbitrary media", *Micr. Optic. Technol. Lett.*, vol. 27, pp. 334-339, 2000.
- [37] S.A. Cummer, "A Simple, nearly perfectly matched layer for general electromagnetic media", *IEEE Micr. Wir. Comp. Lett.*, vol. 13, pp. 128-130, 2003.
- [38] W. Hu, S.A. Cummer, "The nearly perfectly matched layer is a perfectly matched layer", *IEEE Ant. Wir. Propag. Lett.*, vol. 3, pp. 137-140, 2004.
- [39] J.-P. Bérenger, "On the reflection from Cummer's nearly perfectly matched layer", *IEEE Micr. Wir. Comp. Lett.*, vol. 14, pp. 334-336, 2004.
- [40] J.-P. Bérenger, "Evanescent waves in PML's: Origin of the numerical reflection in wave-structure interaction problems", *IEEE Trans. Ant. Propag.*, vol. 47, pp. 1497-1503, 1999.
- [41] W.C. Chew, J.M. Jin, "Perfectly matched layer in the discretized space: an analysis and optimization", *Electromagnetics*, vol. 16, pp. 325-340, 1996.
- [42] J.-P. Bérenger, *Software "Numerical Reflection from PMLs"*: <http://www.morganclaypool.com/page/berenger> or <http://fdtd.perso.sfr.fr/JPB/index%20-%20copy%20-%20copy.htm>.

- [43] J.-P. Bérenger, "Perfectly matched layer for the FDTD solution of wave-structure interaction problems", *IEEE Trans. Ant. Propag.*, vol. 44, pp. 110-117, 1996.
- [44] J.-P. Bérenger, "Making use of the PML absorbing boundary condition in coupling and scattering FDTD computer codes," *IEEE Trans. Electrom. Compat.*, vol. 45, pp. 189-197, 2003.
- [45] J. De Moerloose, M. A. Stuchly, "Behaviour of Berenger's ABC for evanescent waves", *IEEE Micr. Guid. Wav. Lett.*, vol. 5, pp. 344-346, 1995.
- [46] J.-P. Bérenger, "Numerical reflection of evanescent waves from perfectly matched layers", *Proc. IEEE Ant. and Propagat. Symp.*, Montreal, Canada, vol. 2, pp. 1888-1891, July 1997.
- [47] J.-P. Bérenger, "Numerical reflection from FDTD-PML's : A comparison of the split PML with the unsplit and CFS PML's", *IEEE Trans. Ant. Propag.*, vol. 50, pp. 258-265, 2002.
- [48] M. Kuzuoglu, R. Mittra, "Frequency dependence of the constitutive parameters of causal perfectly matched absorbers", *IEEE Micr. Guid. Wave Lett.*, vol. 6, pp. 447-449, 1996.
- [49] J.-P. Bérenger, "Application of the CFS PML to the absorption of evanescent waves in waveguides", *IEEE Micr. Wir. Comp. Lett.*, vol. 12, pp. 218-220, 2002.
- [50] J.-P. Bérenger, "Application of the CFS PML to the FDTD solution of wave structure interaction problems", *Proc. IEEE Ant. Propagat. Symp.*, Columbus, Ohio, vol. 2, pp. 984 - 987, July 2003.
- [51] S.V. Tsynkov, "Artificial boundary conditions for the numerical simulation of unsteady acoustic waves", *J. Comput. Phys.*, vol. 189, pp. 626-650, 2003.
- [52] S.V. Petropavlovsky, S.V. Tsynkov, "A non-deteriorating algorithm for computational electromagnetism based on quasi-lacunae of Maxwell's equations", *J. Comput. Phys.*, vol. 231, pp. 558-585, 2012.
- [53] W. Sudiarta, "An absorbing boundary condition for FDTD truncation using multiple absorbing surfaces", *IEEE Trans. Ant. Propag.*, vol. 51, pp. 3268-3275, 2003.
- [54] R.E. Diaz, I. Scherbatko, "A simple stackable re-radiating boundary condition (rRBC) for FDTD", *IEEE Ant. Propag. Magazine*, vol. 46, pp. 124-130, 2004.
- [55] R.E. Diaz, I. Scherbatko, "A new multistack radiation boundary condition for FDTD based on self-teleportation of fields", *J. Comput. Phys.*, vol. 203, pp. 176-190, 2005.
- [56] J.-P. Bérenger, "On the Huygens absorbing boundary conditions for electromagnetics", *J. Comput. Phys.*, vol. 226, pp. 354-378, 2007, doi: 10.1016/j.jcp.2007.04.008176-190.
- [57] F. Costen, J.-P. Bérenger, "Implementation of the Huygens absorbing boundary condition in corner regions", *IEEE Trans. Electrom. Compat.*, vol. 54, pp. 367-374, 2012.
- [58] J.-P. Bérenger, H. Almeer, F. Costen, "The stretched-mesh Huygens absorbing boundary condition (SM-HABC)", *IEEE Trans. Ant. Propag.*, vol. 62, pp. 3100-3107, 2014, doi: [10.1109/TAP.2014.2314295](https://doi.org/10.1109/TAP.2014.2314295).
- [59] J.-P. Bérenger, "On the general solution of the Maxwell equations and the impact on the absorbing boundary conditions". Workshop "Present challenges in electromagnetic modelization", Saint-Malo, France, Dec. 2-3, 2010.
- [60] J.L. Volakis, A. Chatterjee, L.C. Kempel, *Finite Element Method for Electromagnetics*, IEEE Press, 1998.
- [61] M. Levy, *Parabolic Equation Methods for Electromagnetic Wave Propagation*, IEE Electromagnetic Waves Series, 2000.



Jean-Pierre Bérenger received a Master in Physics from the University Joseph Fourier, Grenoble, France, in 1973, and a Master in Optical Engineering from the Institut d'Optique Graduate School, Paris, France, in 1975.

He has been with the French Ministry of Defense from 1975 to 2013, where he held such positions as research engineer, expert on the electromagnetic effects of nuclear bursts, and contract manager. His technical works were mainly focused on the nuclear electromagnetic pulse and on the propagation of radiowaves in nuclear environments. In this framework he performed researches in the field of numerical electromagnetics, including the FDTD method, the absorbing boundary conditions, and the low frequency (VLF-LF) propagation.

Jean-Pierre Bérenger is currently a consultant on electromagnetic effects of nuclear rays and on numerical electromagnetics, and a visiting professor at the School of Electrical and Electronic Engineering, the University of Manchester, UK. He is a member of the Electromagnetics Academy and has been an Associate Editor of the IEEE Transactions on Antennas and Propagation from 2006 to 2010. He is a Fellow of IEEE and he received the 2013 Medal of URSI-France and the 2014 John Howard Dellinger Gold Medal from URSI.